AGU PUBLICATIONS

Tectonics

RESEARCH ARTICLE
10.1002/2017TC004638

Special Section:
Orogenic cycles: from field observations to global geodynamics

Zircon U-Pb Dating of a Lower Crustal Shear Zone: A Case Study From the Northern Sector of the Ivrea-Verbano Zone (Val Cannobina, Italy)

A. Langone[1], A. Zanetti[1], N. R. Daczko[2], S. Piazolo[3], M. Tiepolo[1,4], and M. Mazzucchelli[1,5]

[1]Istituto di Geoscienze e Georisorse-C.N.R. U.O.S. of Pavia, Pavia, Italy, [2]Australian Research Council Centre of Excellence for Core to Crust Fluid Systems (CCFS)/GEMOC, Department of Earth and Planetary Sciences, Macquarie University, Sydney, New South Wales, Australia, [3]School of Earth and Environment, University of Leeds, Leeds, UK, [4]Dipartimento di Scienze della Terra "A. Desio", Università degli Studi di Milano, Milan, Italy, [5]Dipartimento di Scienze Chimiche e Geologiche, Università degli Studi di Modena e Reggio Emilia, Modena, Italy

Abstract A geochronological study was performed on zircon grains from a middle-lower crustal shear zone exposed in the northern sector of the Ivrea-Verbano Zone (Southern Alps, Italy) for the first time. The shear zone developed at the boundary between mafic rocks of the External Gabbro unit and ultramafic rocks of the Amphibole Peridotite unit. It is ~10–20 m wide, can be followed along a NE strike for several kilometers, and consists of an anastomosing network of mylonites and ultramylonites. Zircon grains were studied in thin sections and as separates from three representative outcrops along the shear zone. Zircon grains are more abundant in the shear zone compared to wall rocks and are generally equant, rounded to subrounded with dimensions up to 500 μm. U-Pb data are mainly discordant, and the apparent $^{206}Pb/^{238}U$ dates show a large variation from Permian to Jurassic. Isotopic data, combined with microstructural, morphological, and internal features of zircon, reveal an inherited age component and suggest partial zircon recrystallization under high-temperature conditions during Late Triassic to Early Jurassic. High-temperature deformation in the shear zone, at lower crustal levels, was coeval with amphibolite to greenschist facies mylonitic deformation at upper crustal levels and is inferred to be related to Mesozoic rifting processes at the Adriatic margin.

Key Points:
- Lower crustal high-temperature deformation is Late Triassic to Early Jurassic
- Large-scale shear zones at different crustal levels were coeval
- Zircon U-Pb dating of mylonitic mafic rocks provides the first evidence of lower crustal deformation associated with Mesozoic rifting

Supporting Information:
- Supporting Information S1
- Table S2
- Table S3
- Table S4

Correspondence to:
A. Zanetti,
zanetti@igg.cnr.it

Citation:
Langone, A., Zanetti, A., Daczko, N. R., Piazolo, S., Tiepolo, M., & Mazzucchelli, M. (2018). Zircon U-Pb dating of a lower crustal shear zone: A case study from the northern sector of the Ivrea-Verbano Zone (Val Cannobina, Italy). *Tectonics*, *37*, 322–342. https://doi.org/10.1002/2017TC004638

Received 21 APR 2017
Accepted 13 DEC 2017
Accepted article online 9 JAN 2018
Published online 31 JAN 2018

1. Introduction

The Ivrea-Verbano zone (IVZ) represents an uplifted part of the pre-Alpine middle to lower continental crust located in the Southern Alps of northwest Italy (e.g., Fountain, 1976; Schmid, 1993). The IVZ and the adjacent Serie dei Laghi (SdL) unit record a long-lasting, ca. 300 Myr, tectono-metamorphic and magmatic history. It represents a natural laboratory useful to understand (i) Paleozoic Variscan metamorphic and magmatic processes, (ii) post-orogenic magmatic underplating and associated lithospheric stretching and thinning, (iii) Mesozoic extension, and (iv) Alpine collisional tectonism (e.g., Handy et al., 1999). Studying the IVZ can aid in the interpretation of present-day deep, lower crustal seismic profiles (Rutter et al., 1993), as well as to understand the connection and/or interplay of structures from the middle to the lower crust. According to the recent work of Beltrando et al. (2015), the IVZ represents part of a complex polyphase rift system, that is, the former western edge of the Adriatic Plate, displaying a well-known episode of rift focusing (e.g., Berra et al., 2009; Bertotti et al., 1993). The timing of the main extensional activity along this fossil passive margin is still under debate. According to several authors, after the early Permian thermal peak, the whole crustal section underwent cooling and exhumation (e.g., Brodie et al., 1989; Siegesmund et al., 2008). Recent studies suggest that the cooling and exhumation history of the IVZ was interrupted by discrete Triassic-Jurassic heating events, as documented by zircon, monazite, and rutile U-Pb dating (Ewing et al., 2015; Langone et al., 2017; Schaltegger et al., 2015; Smye & Stockli, 2014; Vavra et al., 1999; Vavra & Schaltegger, 1999; Zanetti et al., 2013, 2016). Based on the U-Pb dating of rutile from the high-grade metamorphic rocks (granulites) of the central and southern part of the IVZ, some authors suggest that discrete regional-scale thermal pulses affected the lower structural levels of the IVZ in response to the Mesozoic hyperextension associated with rift/post-rift processes at the Adriatic margin (Ewing et al., 2015; Smye & Stockli, 2014). While a network of conjugate, high-temperature, low-angle shear zones that developed at granulite to amphibolite facies conditions has been recognized (Rutter et al., 1993; Rutter et al., 2007), it remains unclear if these are directly related to the proposed Mesozoic heating associated with rifting and exhumation. The available Ar-Ar

dating were interpreted as indicative of Permian deformation in the shear zones with Triassic perturbation of the isotopic system (e.g., Brodie et al., 1989) or as the maximum age of synkinematic recrystallization (Boriani & Villa, 1997). According to Beltrando et al. (2015), the available Ar-Ar data are best explained as arising from post-Permian, likely Triassic-Jurassic, amphibole recrystallization.

Here we present new chemical and isotopic zircon data from a high-temperature shear zone developed in meta-basic rocks of the northeastern IVZ sector. We discuss the role of the studied shear zone at crustal and regional scales and its possible connection with other lower crustal shear zones, in the framework of a fossil-rifted margin.

2. Geological Setting

The IVZ in northwestern Italy (e.g., Schmid, 1993; Figure 1a) extends for about 120 km and is bounded by two major fault zones, the Insubric Line in the northwest and the Cossato-Mergozzo-Brissago Line in the southeast (Figure 1a). The latter was active in the Late Carboniferous and Early Permian and was reactivated also during Triassic (Boriani et al., 1990, Boriani & Villa, 1997; Mulch, Cosca, et al., 2002; Klötzli et al., 2014). Locally, the Cossato-Mergozzo-Brissago mylonites are crosscut and partially overprinted by mylonites of the Pogallo Line (Figure 1a), which is interpreted as a low-angle normal fault that formed during crustal thinning (Hodges & Fountain, 1984) in Triassic-Jurassic time (210–170 Ma; Zingg et al., 1990).

The central/southern part of the IVZ (e.g., Val Sesia) has been traditionally subdivided into three main rock units: Kinzigite Formation (amphibolite- to granulite-facies metamorphic rocks), Mafic Complex (intrusive mafic rocks; Figure 1a), and mantle peridotite. These units strike SW-NE, and metamorphic grade increases from amphibolite to granulite facies toward the NW (e.g., Demarchi et al., 1998; Henk et al., 1997; Redler et al., 2012; Schmid, 1993; Schmid & Wood, 1976; Zingg, 1983). The Kinzigite Formation occupies the southeastern and originally upper part of the tilted crustal section (Figure 1a). It consists of siliciclastic metasedimentary rocks with intercalated meta-basic rocks and minor calcsilicate rocks and marble. The regional metamorphic assemblages are overprinted by contact metamorphism near gabbroic rocks of the Mafic Complex (e.g., Barboza & Bergantz, 2000, Barboza et al., 1999; Redler et al., 2012; Figure 1a). The Mafic Complex consists of gabbro, norite, and diorite (e.g., Rivalenti et al., 1975; Sinigoi et al., 2010) and was emplaced during the Permian (e.g., Peressini et al., 2007).

The northernmost sector of the IVZ (i.e., Val Cannobina; Figures 1a and 1b) is characterized by a lens-shaped structure made of mantle peridotite (Phlogopite Peridotite) in the core and surrounded by intrusive crustal mafic to ultramafic rocks, the Finero Mafic Complex. The latter shows significant differences in terms of petrochemical and structural features compared with the Mafic Complex in the south and consists of three different units (Siena & Coltorti, 1989): (i) the Layered Internal Zone (garnet-hornblendite, pyroxenite, anorthosite, and garnet-bearing gabbro); (ii) the Amphibole Peridotite, and (iii) the External Gabbro, which is in contact with the metamorphic sequence of the Kinzigite Formation toward the SW (Figures 1b and 1c). The whole mafic/ultramafic sequence (mantle peridotite and the Finero Mafic Complex) is crosscut by pegmatitic dykes and pods intruded mainly from Triassic to Jurassic time within peridotites and ultramafic rocks (e.g., Frenzel et al., 1990; Grieco et al., 2001; Hingerl et al., 2008; Klotzli et al., 2007; Schaltegger et al., 2015; Stähle et al., 2001; von Quadt et al., 1993) and during Carboniferous-Permian within the External Gabbro unit (Langone et al., 2017).

The External Gabbro unit is 400–500 m thick and mainly consists of amphibole (±garnet) gabbro and diorite, with minor pyroxenite and anorthosite bands (e.g., Hingerl et al., 2008). According to recent U-Pb zircon dating, intrusion took place at lower crustal levels in several pulses from the Permian to Triassic (e.g., Langone et al., 2017; Zanetti et al., 2013). Several slivers or lenses ($<$1 m to 100 m thick) of granulite from the Kinzigite Formation occur within the External Gabbro unit and are referred to as septa (Rivalenti et al., 1975).

The rocks of the External Gabbro unit show metamorphic textures suggesting re-equilibration under granulite facies conditions and are characterized by pervasive brittle-ductile deformation features (e.g., Boriani et al., 1990; Langone & Tiepolo, 2015). Ductile deformation varies from well-developed mylonitic fabrics to S-type shear bands. An ultramylonitic/mylonitic belt defines the contact between the External Gabbro unit and the underlying Amphibole Peridotite unit (Figures 1b and 1c; Kenkmann, 2000, Stähle et al., 2001;

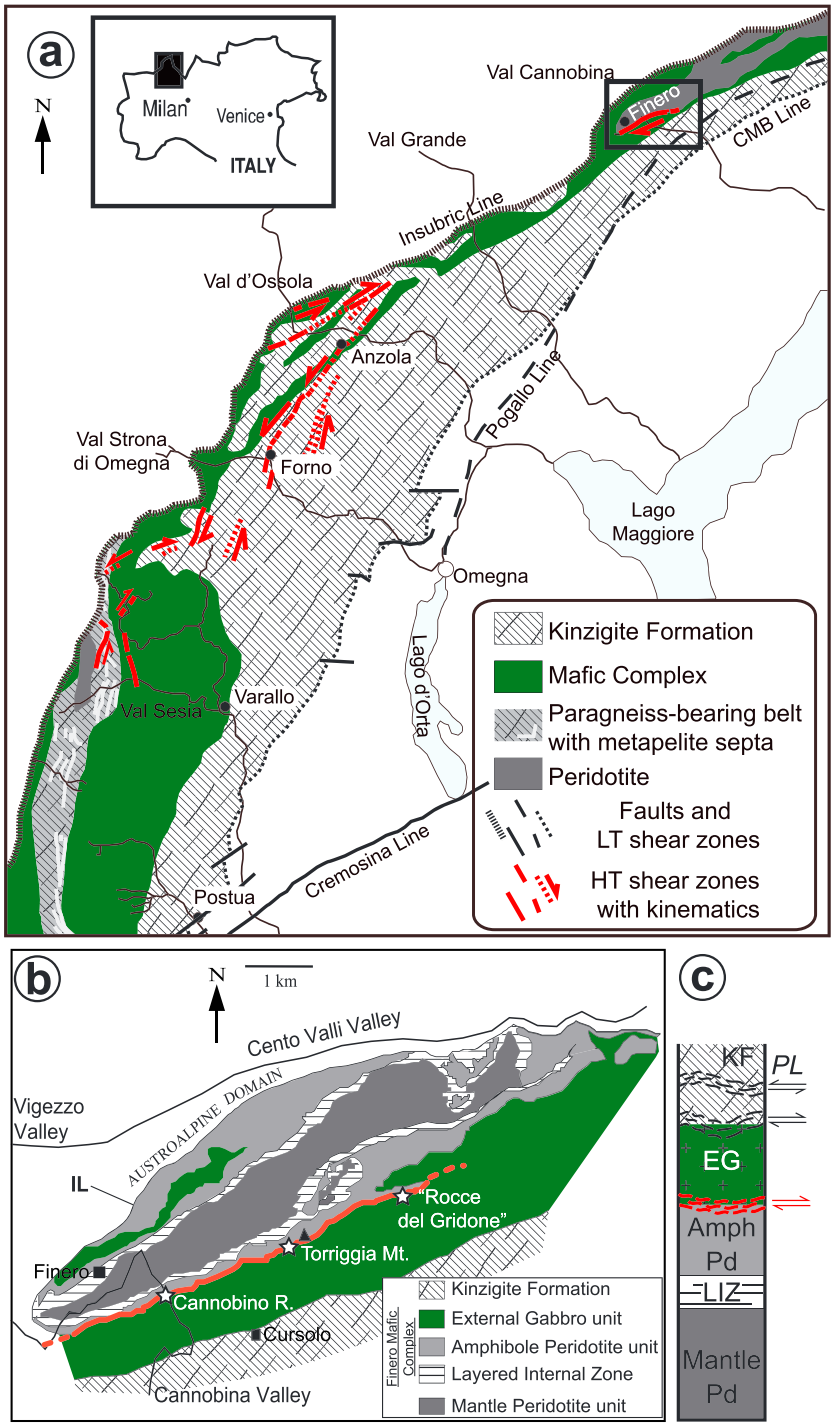

Figure 1. (a) Geological sketch map of the central and northern IVZ (modified after Ewing et al., 2015). The locations of high-temperature shear zones are after Rutter et al. (1993). (b) Sketch map of the northern sector of the Ivrea-Verbano zone. (c) Schematic section (not to scale) from mantle to crustal rocks showing the location of the studied shear zone (red) and other shear zones reported on the geological map of Boriani and Burlini (1995; PL = Pogallo Line).

Langone & Tiepolo, 2015). Ductile deformation occurred at $T \geq 650$°C and $P \geq 0.6$–0.4 GPa (Degli Alessandrini et al., 2016) and continued under retrograde conditions at $T = 650$–500°C and $P = 0.6$–0.4 GPa (Kenkmann, 2000; Kenkmann & Dresen, 2002). This is the first study to date the shear zone using zircon. However, using Ar-Ar dating of amphibole, Boriani and Villa (1997) suggested that mylonitization of hornblendite

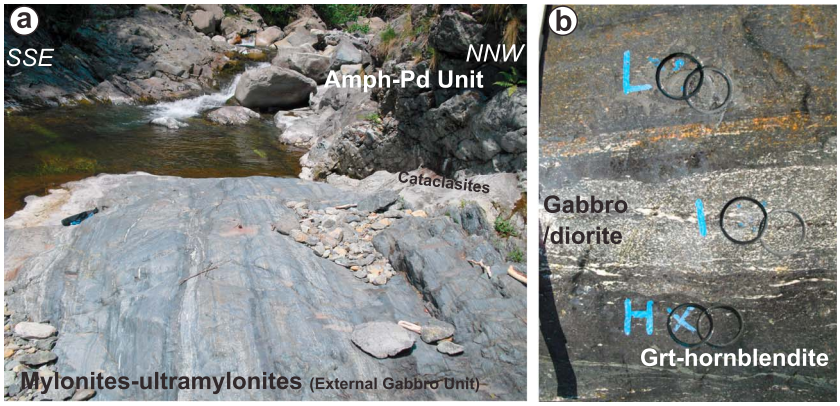

Figure 2. (a) Photograph of the Cannobino River outcrop showing the mylonitic/ultramylonitic belt and the cataclasites toward the contact with the Amph-Peridotite unit. (b) Photograph showing the main lithological variations of the mylonites/ultramylonites. The picture also shows the locations of some 1 inch drill cores collected for both petrological and geochronological investigations.

and gabbro of the External Gabbro unit took place from 220 to 180 Ma, based on a mylonitic hornblende (sampled from the tunnel south of the Finero village; Figures 1a and 1b) dated at 183.3 ± 1.9 Ma.

3. Field Observations, Petrography, and Microstructures

The studied shear zone consists of mainly gray, dark-gray mylonites, and ultramylonites that strike SW-NE and show a subvertical to high-dip attitude (Figure 2). The mylonitic/ultramylonitic belt, reported on the geological map of the Cannobino Valley by Boriani and Burlini (1995), can be followed for several kilometers from the Cannobino River (SW) toward the "Rocce del Gridone" (NE; Figure 1b). The Cannobino River outcrop is the most studied (e.g., Degli Alessandrini et al., 2016; Kenkmann, 2000; Kenkmann & Dresen, 2002; Stähle et al., 2001) and shows the sheared contact between the Amphibole Peridotite unit and the External Gabbro unit. Toward the Amphibole Peridotite unit, a meter-thick cataclastic band occurs and consists of fine-grained light-gray cataclasite with fragments of deformed peridotites, pyroxenites, and gabbroic rocks (Figure 2). The core of the shear zone is characterized by finely spaced mylonites in compositionally banded rocks (Figures 2b and 3a–3f). Along the river, the rocks are polished by the water, and lithological variations and microstructural elements can be more easily followed (Figure 2b). The deformed amphibole gabbro/diorite is the main rock type, whereas coarse-grained garnet-hornblendite mylonites are less common. Locally, deformed leucocratic rocks, consisting of plagioclase and garnet, occurs (Figures 3a, 3b, 3e, and 3f). On the polished outcrop surfaces, plagioclase-rich mylonitic layers are easily distinguishable from other mafic rocks, as well as layers consisting of rounded reddish garnet porphyroclasts embedded in a fine-grained matrix. Dark-gray ultramylonitic layers are also common.

The mylonitic/ultramylonitic belt is about 10 m thick and grades structurally upward into mylonites and poorly deformed gabbroic rocks. The transition from mylonites to undeformed gabbroic rocks is characterized by anastomosing shear planes and S-C′ bands. Along the shear zone, centimeter-thick pseudotachylite veins occur. They are increasingly more common in the NE outcrops (i.e., Torriggia Mt. and "Rocce del Gridone"; Figures 1b and 3f) and generally are continuous over a few meters. In some cases, they define a breccia-like network.

Different samples from the shear zone were investigated for petrography and microstructures: 15 drill cores with a diameter of 1 inch were collected from the polished surface of the Cannobino River outcrop (Figure 2b), whereas hand specimen samples were collected along the shear zone (Figure 1b). Thin section analysis shows that compositional variation occurs not only at the outcrop but also at the microscale (Figures 1 and 3). Intercalating bands of different composition vary from a few millimeters to about 2 cm in thickness (Figure 3). The deformed amphibole (±garnet) gabbro/diorite (Figures 3a, 3b, 3e, and 3f) consists of hornblende, two pyroxenes, and plagioclase with or without garnet, whereas the coarse-grained garnet-hornblendite mylonite layers are made of large brown amphibole and garnet crystals with or without

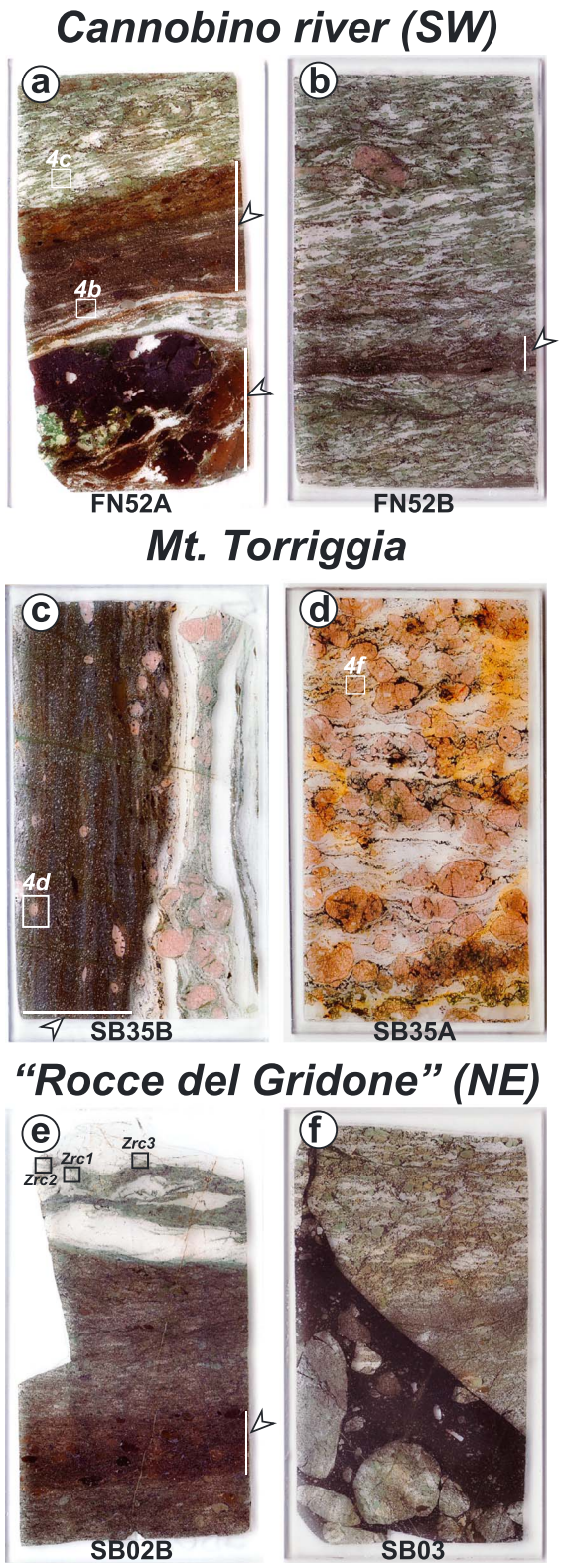

Figure 3. Optical scan of thin sections from the three studied outcrops: (a and b) Cannobino River (FN52A and FN52B); (c and d) Torriggia Mt. (SB35B and SB35A); "Rocce del Gridone" (SB02B and SB03). Arrows indicate garnet-hornblenditic layers. White boxes in Figures 3a–3d delimit the location of pictures in Figure 4; in Figure 3e, the location of zircon grains is also reported.

clinopyroxene and plagioclase. Accessory minerals such as apatite and zircon are common in both rock types, whereas titanite locally occurs. Oxides and sulfides are also common. Generally, hornblende, pyroxenes, and locally garnet occur as porphyroclasts surrounded by a fine-grained matrix consisting mainly of amphibole and plagioclase. Amphibole porphyroclasts show variable shape and dimensions from subhedral grains to rounded and/or highly elongated grains (aspect ratios up to 8; Figure 4b). They can have an overgrowth of a lower temperature mineral such as a secondary amphibole and/or epidote and can also be surrounded by oxides (Figure 4a). Plagioclase porphyroclasts show intracrystalline deformation features (undulose extinction, deformation twins, and irregular grain boundaries), which are absent where plagioclase occurs as an inclusion in garnet or amphibole. Pyroxenes are partially to totally replaced by secondary minerals such as amphibole, serpentine, and/or epidote; replacement is mainly seen along grain boundaries and brittle fractures crossing individual grains or along cleavages. Relicts of clinopyroxene are more common than those of orthopyroxene. Partially replaced clinopyroxene commonly shows lamellae of amphibole parallel to the cleavage planes and along fractures (e.g., Kenkmann, 2000) that are commonly at a high angle with respect to the mylonitic foliation. Clinopyroxene porphyroclasts can show undulose extinction and deformation (kinks) of the cleavage planes (Figure 4a). Within the shear zone, garnet abundance is highly variable; it can be rare or reach a modal abundance up to 60 vol.%. Garnet forms millimeter-sized porphyroclasts with rounded (Figure 4d) or highly elongated shapes (aspect ratio up to 4.5). It can be totally or partially surrounded by symplectite consisting of mainly plagioclase and orthopyroxene (e.g., Degli Alessandrini et al., 2016). Garnet shows a dense network of fractures and can be partially or totally replaced by secondary minerals, that is, chlorite and epidote (Figure 4e). Within the plagioclase- and garnet-rich mylonitic metadiorite, garnet is rarely partially surrounded by a fine-grained aggregate of sillimanite. Garnet can contain inclusions of amphibole, two pyroxenes, plagioclase, oxides, and zircon (Figure 4e). Biotite, titanite, and epidote are also common along the mylonitic foliation planes documenting the retrograde evolution in greenschist facies defined by the assemblage chlorite, actinolite, epidote, and albite.

4. Analytical Methods

Zircon grains from different samples collected along the shear zone were characterized in terms of internal zoning and chemical and isotopic composition directly on thin section and as mineral separates. A zircon separate (>200 grains) was obtained from one large meta-diorite/gabbro sample (>2 kg) from the Cannobino River outcrop. After sample crushing, zircon grains were separated using a Frantz magnetic separator and heavy liquids and then mounted in epoxy and polished.

A summary including sample type, location, geographic coordinates, the number of analyzed grains, the analytical approach (separates versus thin section), and the type of characterization is reported in Table 1.

4.1. Internal Zonation Revealed by Cathodoluminescence

Prior to isotopic characterization of zircon grains, their textural position and internal features were imaged with scanning electron microscopes

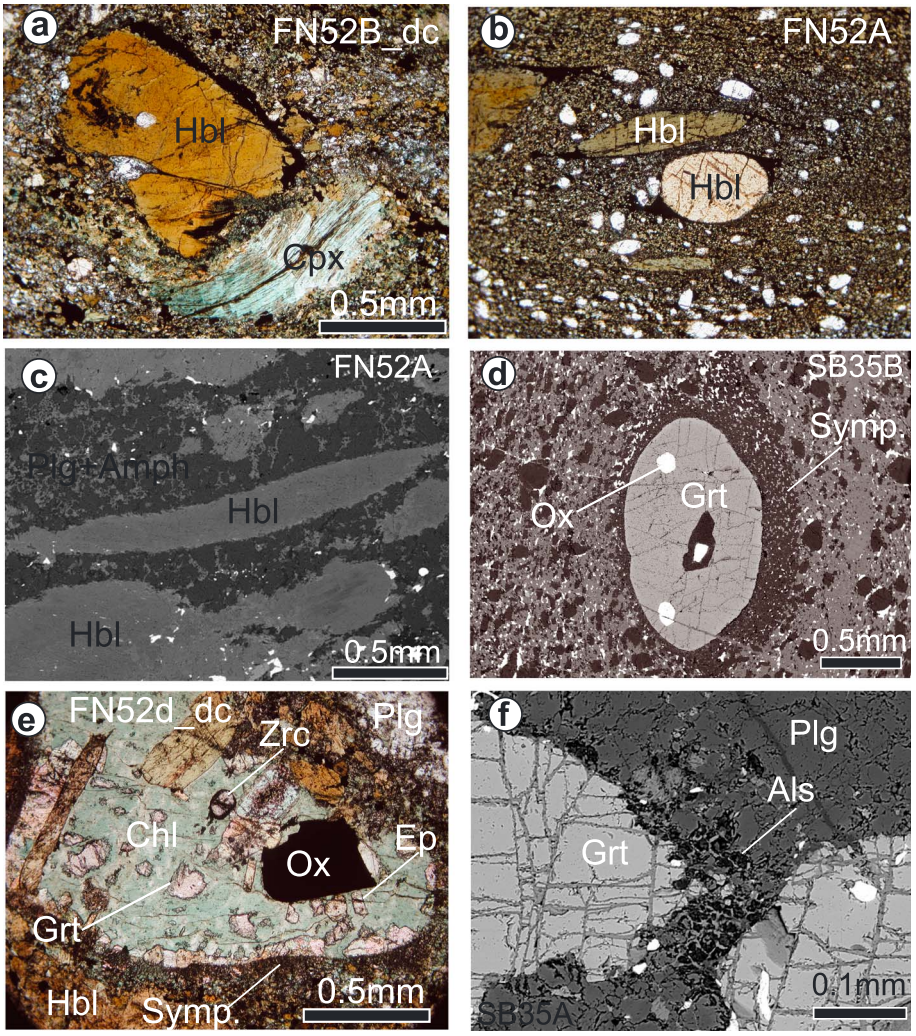

Figure 4. (a) Brown-hornblende and clinopyroxene porphyroclasts from a hornblenditic layer (FN52A, Cannobino River). (b) Sigma-type porphyroclasts of hornblende surrounded by a fine-grained matrix consisting mainly of amphibole and plagioclase. Small porphyroclasts of plagioclase are also recognizable (SB35B). (c) SEM-backscattered electron (BSE) image of a highly elongated porphyroclasts of hornblende showing brighter overgrowths of a new amphibole (FN52A). (d) SEM-BSE image of rounded garnet porphyroclasts surrounded by a fine-grained symplectite of plagioclase + orthopyroxene (SB35A). (e) Large garnet grain almost completely replaced by chlorite and epidote. Garnet contains inclusions of oxides and zircon. An asymmetric symplectitic corona is also visible. (f) SEM-BSE image showing two garnet porphyroclasts within the plagioclase-rich matrix and partially surrounded by tiny aluminosilicates (SB35A). Abbreviations after Kretz (1983).

Table 1
List of Analyzed Samples With Their Coordinates and Summary of the Analytical Approach

	Locality	Sample name	Analyzed Zrc grains	LA-ICP-MS analyses			LA-MC-ICP-MS
				U-Pb 25 μm	U-Pb 10 μm	Trace element	Hf isotopes
SW	Cannobino River, 46°6′8.77″N, 8°32′47.32″E, 810 m.a.s.l.	FN52 separates	75	103	36	v	v
		FN52A (1″ thin section)	7	12			
		FN52B (1″ thin section)	4	9			
		FN52B (regular thin section; see Figure 3b)	7	12			
	Torriggia Mt., 46°6′40.87″N, 8°34′30.13″E, 1,555 m.a.s.l.	SB35A (regular thin section; see Figure 3d)	23	39		v	
NE	"Rocce del Gridone," 46°7′7.91″N, 8°35′57.99″E, 1,696 m.a.s.l.	SB02B (regular thin section; (see Figure 3e)	3	14		v	

(SEMs) (Figures 5–8). The textural positions of zircon were studied with the field emission (FE)-SEM Mira3 Tescan hosted at the Dipartimento di Scienze della Terra e dell'Ambiente of Pavia. The FE-SEM was operated at 20 kV and 16 mm working distance. Cathodoluminescence (CL) images were acquired with a SEM Philips 515 equipped with a Centaurus scintillator CL detector at the Consiglio Nazionale delle Ricerche (CNR) Istituto di Geoscienze e Georisorse (IGG), Sezione di Pavia. The SEM was operated at 15 kV and 26 mm of working distance.

4.2. U-Pb Geochronology

U-Pb zircon geochronology was carried out at the CNR-IGG of Pavia with laser ablation–inductively coupled plasma–mass spectrometry (LA-ICP-MS). The system couples an ArF excimer laser microprobe (type GeoLas102 from MicroLas) with a sector field ICP-MS (type Element from ThermoFinnigan). The signals of ^{202}Hg, ^{204}(Pb + Hg), ^{206}Pb, ^{207}Pb, ^{208}Pb, ^{232}Th, and ^{238}U masses were acquired. ^{202}Hg is acquired to correct the isobaric interference of ^{204}Hg on ^{204}Pb, so that the presence of common Pb in the sample can be monitored. However, the background of mass 204 is relatively high, due to traces of Hg in the He gas, and therefore, small amounts of common Pb are below detection limits. In the investigated samples, the signal of ^{204}(Pb + Hg) was always indistinguishable from the background. The ^{235}U signal is calculated from ^{238}U based on the ratio ^{238}U/^{235}U = 137.818 (Hiess et al., 2012). U-Pb fractionation effects in zircon were simultaneously corrected using a matrix matched external standard and considering the same integration intervals on the standard and the unknowns. Analyses were carried out using spot sizes of 25 and 10 μm, a repetition rate of 5 Hz, and a laser fluence of 8 J cm^{-2}. The reference zircon GJ-1 (609 Ma; Jackson et al., 2004) was adopted as external standard, and the reference zircons 91500 (1,065 Ma; Wiedenbeck et al., 1995) and/or 02123 (295 Ma; Ketchum et al., 2001) were selected as validation standards. Precision (relative standard deviation) and accuracy (percent error) are better than 2% and 5% for 91500 reference zircon and 1% and 2% for 02123 reference zircon. Data reduction was carried out with the software package GLITTER® (Van Achterbergh et al., 2001). The relative standard deviation of ^{207}Pb/^{206}Pb, ^{206}Pb/^{238}U, and ^{207}Pb/^{235}U ratios of the GJ-1 external standard varies from 0.3% to 2.1% and from 2.2% to 3.8% for analyses at 25 μm and 10 μm, respectively. Within the same analytical run, the error associated with the reproducibility of the external standard was propagated to each analysis of samples (see Horstwood et al., 2003), and after this procedure, each data determination is retained accurate within the quoted error. The ISOPLOT/Ex 3.00 software package by Ludwig (2003) was used for U-Pb apparent date calculations and representations. Results of zircon and reference materials are reported in Appendix Table A1 in the supporting information.

4.3. Trace Elements

The trace element compositions of zircon grains were analyzed on separate spots by LA-ICP-MS using a quadrupole ICP-MS (type DRCe from PerkinElmer) interfaced to a New Wave UP-213 Nd:YAG laser at the CNR-IGG UOS of Pavia. The ablation system was operated at a 10 Hz repetition rate, 25/35 μm spot size, and with a fluence of ~9 J cm^{-2}. Helium was used as the carrier gas and mixed with Ar downstream of the ablation cell. NIST SRM 610 synthetic glass was used as external standard, whereas Si was adopted as internal standard. Precision and accuracy were assessed from repeated analyses of the NIST SRM 612 standards, and results were usually within 10% of known values. Average element abundances in synthetic glasses NIST SRM 610 and NIST SRM 612 were taken from Pearce et al. (1997). Background and signal were measured for about 50–60 s; the signal of both standards and unknowns were carefully checked, and the raw data were reduced using the software package GLITTER® (Van Achterbergh et al., 2001). Results are reported in Appendix Table A2.

4.4. Ti-in-Zircon Thermometry

Ti-in-zircon thermometry was applied to analyze zircon grains according to the calibration of Watson et al. (2006). The estimated error considers both the analytical uncertainty on Ti measurements (from 15 up to 50%,;Table A2) and the error from the calibration (Watson et al., 2006). The large analytical uncertainty on the Ti measurements are related to the small spot sizes used for the analyses (i.e., 25/35 μm) and locally to the short duration of the signal due to the limited thicknesses of zircon grains/domains.

4.5. Hf Isotopes

In situ Hf isotope analyses were performed on some of the same grains analyzed for U-Pb and trace elements using a New Wave UP-213 Nd:YAG laser ablation microprobe attached to a Nu Plasma multicollector

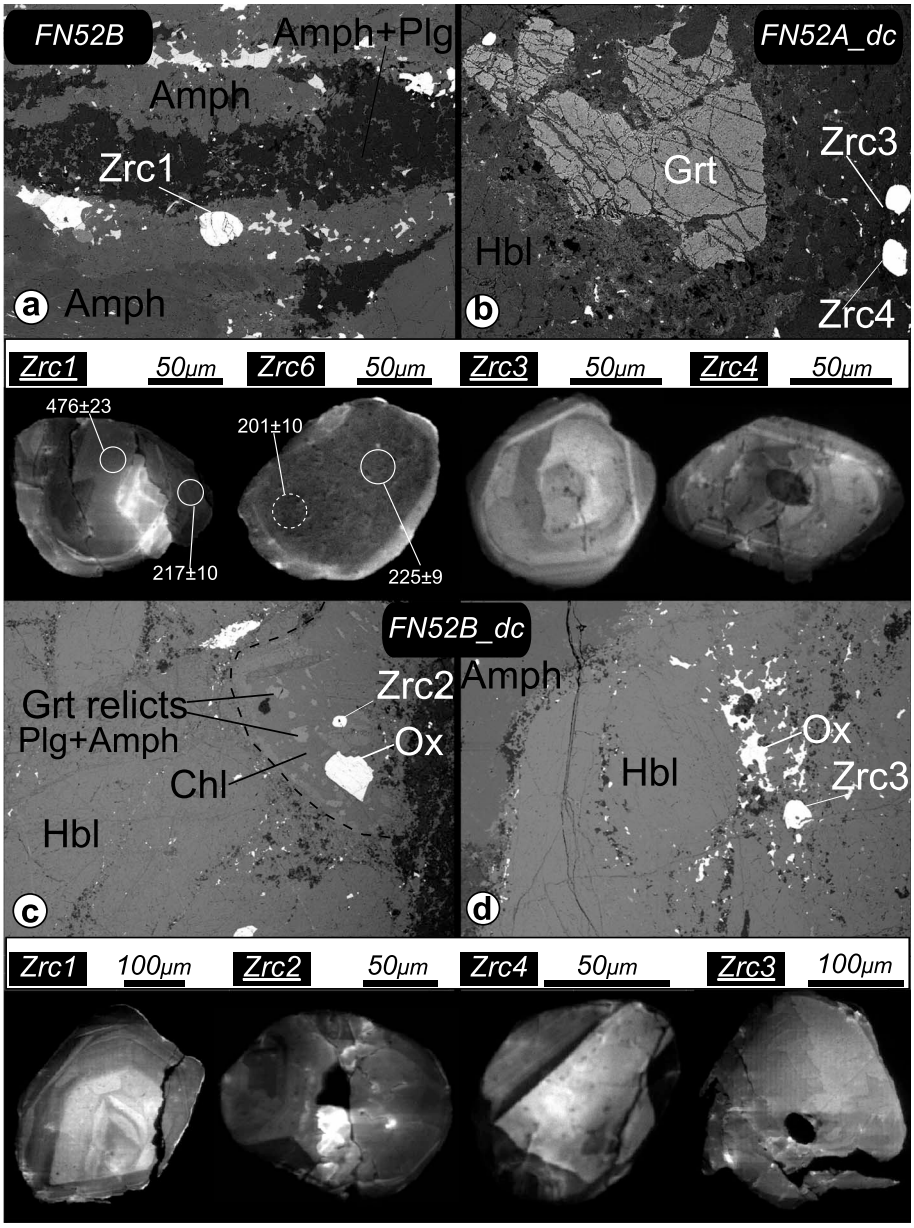

Figure 5. SEM-BSE images showing zircon grains in their textural position within the FN52 samples from the Cannobino River outcrop: (a and b) zircon grains within the matrix, (c) within garnet, and (d) among large hornblendes. CL images of selected and analyzed zircon grains are also reported. Zircon grains with underlined names are those shown in SEM-BSE images in Figures 5a–5d. Location of LA-ICP-MS and obtained U-Pb ages (with associated 2σ error) are also shown on the CL images: white circles = concordant data; white dashed circles = $^{206}Pb/^{238}$ U data.

(MC)-ICP-MS system at Macquarie University. Griffin et al. (2004) describe the methodology in detail. A blank gas was analyzed for 60 s followed by 120 s of ablation at a beam diameter of 40 μm, 5 Hz, and 2 J/cm^2. Zircon CL images were used to guide Hf isotope analyses to be contained within the same domain analyzed for U-Pb. The Mud Tank zircon was used as a reference standard for Hf analysis; our mean $^{176}Hf/^{177}Hf$ value for this zircon is 0.282515 ± 10 (2sd, n = 3) within error of the published value of 0.282522 ± 42 (Griffin et al., 2007). Uncertainties quoted are the internal measured uncertainty and do not include any propagation of error from this reference standard.

The initial $^{176}Hf/^{177}Hf$ (Hf_i) value in zircon is calculated using the measured ^{176}Lu, $^{176}Hf/^{177}Hf$, and $^{206}Pb/^{238}U$ age. The calculation of εHf values used the ^{176}Lu decay constant of Scherer et al. (2001) of 1.865×10^{-11}.

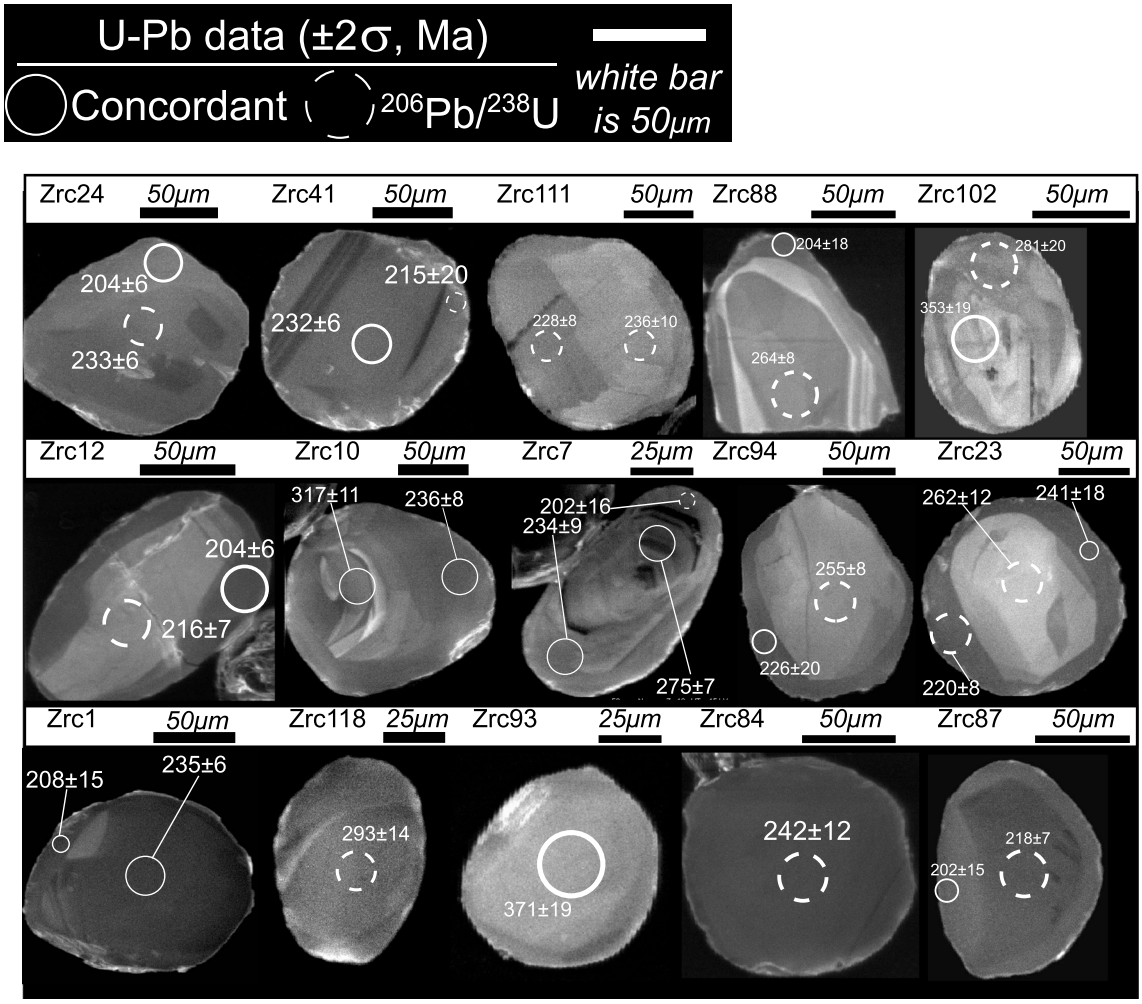

Figure 6. CL images of zircon separates from samples FN52 of the Cannobino River outcrop. Location of LA-ICP-MS and obtained U-Pb data (with associated 2σ error) are also shown on the CL images: white circles = concordant data; white dashed circles = $^{206}Pb/^{238}$ U data.

Model age calculations (T_{DM}) are based on a depleted mantle source with Hf_i = ($^{176}Hf/^{177}Hf$) initial = 0.279718 and $^{176}Hf/^{177}Hf$ = 0.0384. This provides a value of $^{176}Hf/^{177}Hf$ (0.28325) like that of average mid-ocean ridge basalt over 4.56 Ga. The calculated T_{DM} ages use the measured $^{176}Lu/^{177}Hf$ of the zircon and give a minimum age for the source material of the magma from which the zircon crystallized. A "crustal" model age ($T_{DM}^{Hf(c)}$) was also calculated for each zircon grain (at its individual $^{206}Pb/^{238}U$ age); this two-stage calculation assumes that the parental magma was derived from the average continental crust ($^{176}Lu/^{177}Hf$ = 0.015), which in turn was originally derived from the depleted mantle. Data are reported in Appendix Table A3.

5. Zircon Abundance, Microstructures, and Internal Features

Zircon grains are generally abundant, with up to 30 grains per thin section found. For the Cannobino River outcrop, zircon grains were studied in nine thin sections; they are preferentially located in (garnet-)hornblendite (e.g., Figure 5) and leucocratic (plagioclase ± garnet) layers (i.e., Torriggia Mt. outcrop, Figures 3c, 3d, and 7; "Rocce del Gridone" outcrop, Figures 3e and 8).

Zircon grains occur in different textural positions including (1) as inclusions within garnet and amphibole porphyroclasts (Figures 5 and 7), (2) interstitial between porphyroclasts (Figure 5), and (3) within the fine-grained matrix (Figures 5, 7, and 8). Zircon grains occurring as inclusions within garnet

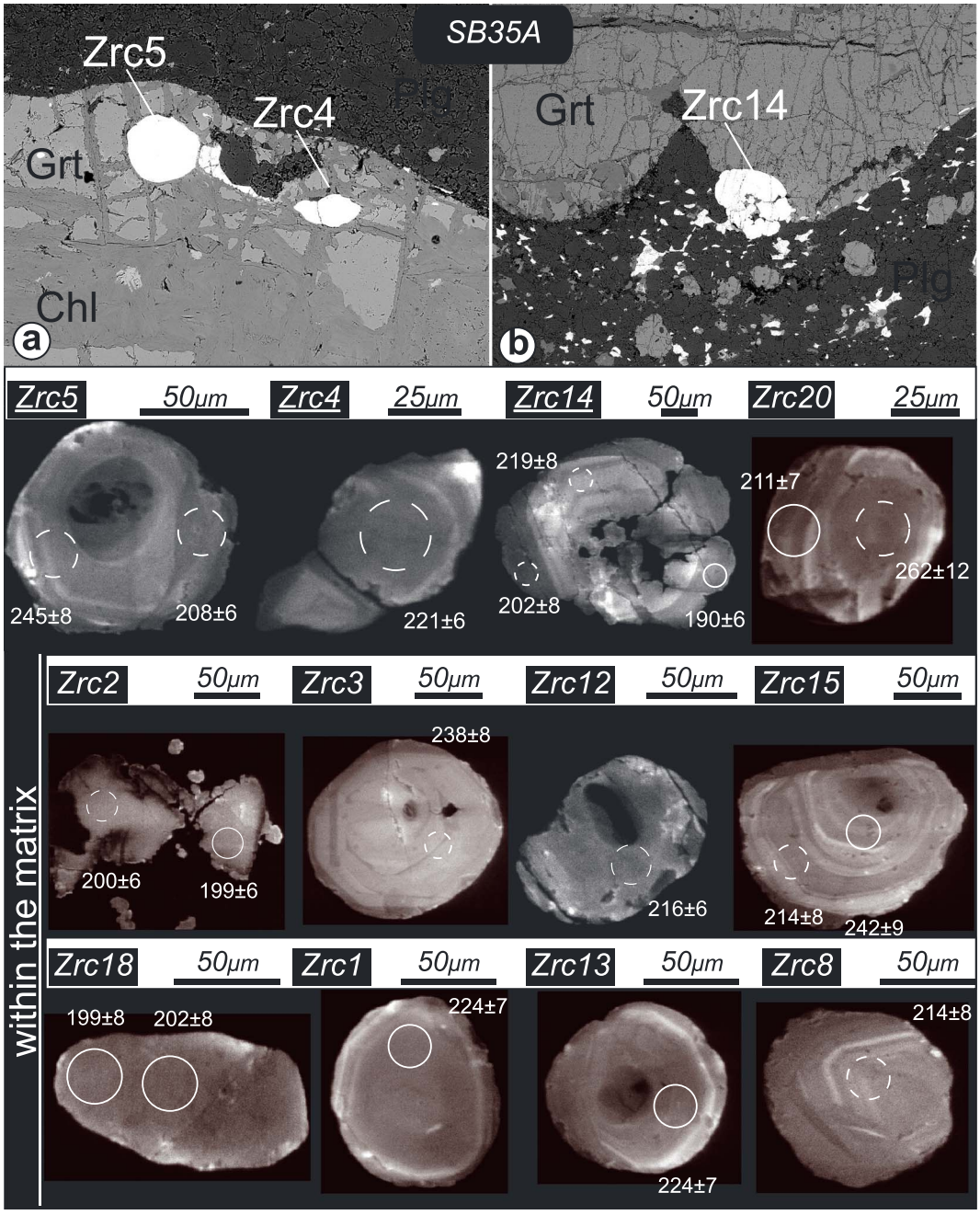

Figure 7. (a and b) SEM-BSE images showing zircon as inclusion within garnet from the SB35A sample of the Torriggia Mt. outcrop. Zircon grains with underlined names are those shown in SEM-BSE images in Figures 7a and 7b. CL images of selected and analyzed zircon grains are also reported. Location of LA-ICP-MS and obtained U-Pb data (with associated 2σ error) are also shown on the CL images: white circles = concordant data; white dashed circles = $^{206}Pb/^{238}$ U data.

porphyroclasts are generally in the rims of the crystals and are always connected with the matrix by fractures (Figures 5 and 7).

Zircon grains commonly show rounded shapes with a mean aspect ratio of 1.2; sigmoidal and elongated shapes also occur (Figure 7). No euhedral grains are present. In a few cases, zircon within the plagioclase-rich matrix of the sample SB35 shows lobate contours defining a cauliflower-like structure (e.g., Zrc14 and Zrc2 in Figure 7). For the "Rocce del Gridone" sample (Table 1), a large zircon grain was observed within the hinge zone of a foliation fold/crenulation (Figures 3e and 8). Grain dimensions are highly variable from a few square micrometers up to 210 × 180 μm (Torriggia Mt.; Figure 7) and

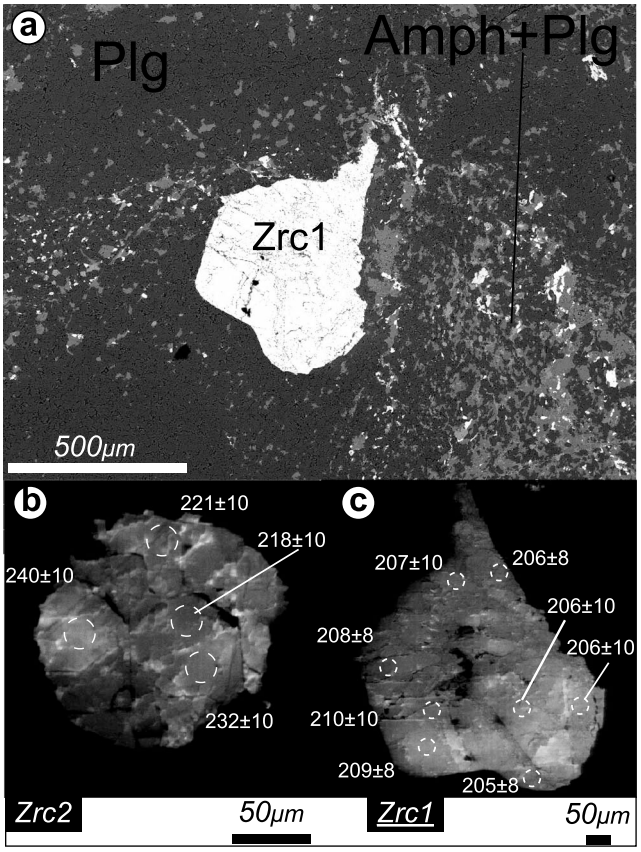

Figure 8. (a) SEM-BSE image showing zircon (Zrc1) within the matrix from the SB02B sample of the "Rocce del Gridone" outcrop. CL images of selected and analyzed zircon grains are also reported. Location of the LA-ICP-MS and obtained $^{206}Pb/^{238}U$ data (with associated 2σ error) are also shown on the CL images: white dashed circles.

400 × 500 μm ("Rocce del Gridone"; Figure 8). Fractures with or without grain displacement are common, especially for zircon within the matrix (e.g., Figure 5; Zrc4 and Zrc14 in Figure 7; and Figures 8b and 8c).

The CL features are variable. Generally, (sub)rounded cores can show homogeneous CL features or oscillatory/sector zoning. These cores can be surrounded by thin (<30 μm), irregular (asymmetric), and homogeneous rims. Large grains showing lobate boundaries and showing dark and homogeneous CL features occur (e.g., Zrc2; Figure 7). The three large zircon grains from the "Rocce del Gridone" sample are intensely fractured, and CL images are characterized by polygons showing different CL emission that appear to overprint pre-existing CL zoning patterns (i.e., sector; Figure 9). For both the Cannobino River and Torriggia Mt. outcrops, no systematic differences of the CL features were observed for zircon within different compositional bands and textural positions.

6. Zircon Isotopes and Chemical Composition

6.1. U-Pb Dating and Trace Elements

6.1.1. Cannobino River Outcrop

A total of 172 analyses were performed on 93 zircon grains. Analyses were mainly performed on zircon separates (138 analyses for 75 zircon grains). U-Pb analyses of zircon in thin sections were performed on three different samples (FN52B, FN52A_dc, and FN52B_dc) for a total of 33 analyses on 18 zircon grains (Table A1). U-Pb data are mainly discordant (62% of analyses) with only 65 concordant data (Figure 9a). These latter define an asymmetric distribution with two main peaks at about 200 and 236 Ma and with a tail toward older data (Figure 9b). The younger cluster of U-Pb concordant data refers mainly to dark homogeneous rims and to structureless domains (e.g., Zrc6 in Figure 5; Zrc24, Zrc88, Zrc7, Zrc12, Zrc1, and Zrc87 in Figure 6); a weighted average of these data was calculated at 202.3 ± 2.2 Ma (MSWD = 0.65; Figure 9b). Older concordant U-Pb data were obtained from zircon grains/domains characterized mainly by sector or oscillatory zoning (e.g., Zrc24, Zrc41, and Zrc111 in Figure 6). Triassic data were obtained also from homogeneous domains (e.g., Zrc1 and Zrc84 in Figure 6) and from domains/overgrowths around older cores showing different CL features (e.g., Zrc1 in Figure 5 and Zrc10, Zrc7, Zrc94, and Zrc23 in Figure 6).

A weak negative Eu anomaly and a marked positive Ce anomaly characterize all analyzed zircon domains (Figure 10). The Th/U ratio ranges between 0.27 and 0.89. The rare earth element (REE) pattern normalized to chondrite (CI; McDonough & Sun, 1995) of the inner homogeneous cores (>240 Ma) are characterized by a strong fractionation between light rare earth element (LREE) and heavy rare earth element (HREE) with the latter up to 1,000 times CI (Table A2; Figure 10a). The internal domains with magmatic (sector and oscillatory) zoning and Middle Triassic U-Pb concordant and $^{206}Pb/^{238}U$ data possess CI normalized REE pattern paralleling that of the homogeneous cores, but at slightly lower absolute values (HREE are up to 700 times CI; Figure 10a). In contrast, REE patterns of the external domains, mostly giving a weighted average age of 202.3 ± 2.2 Ma (Figure 9b), differ for their flat HREE and generally low HREE content (about 100 times CI chondrite). External domains have also slightly lower Th/U ratios (0.21–0.49) with respect to domains showing oscillatory zoning and cores with homogeneous CL features.

Zircon grains show a Ti content ranging from 6.31 to 31.36 ppm (17 data, Table A2), and the estimated temperatures vary from 702 to 853°C (Figure 10d).

6.1.2. Torriggia Mt. Outcrop

A total of 39 analyses were collected for 23 zircon grains from the Torriggia Mt. sample (SB35A; Table A1). The data are mainly discordant (62% of analyses) with only 11 concordant dates ranging from 190 ± 6 to

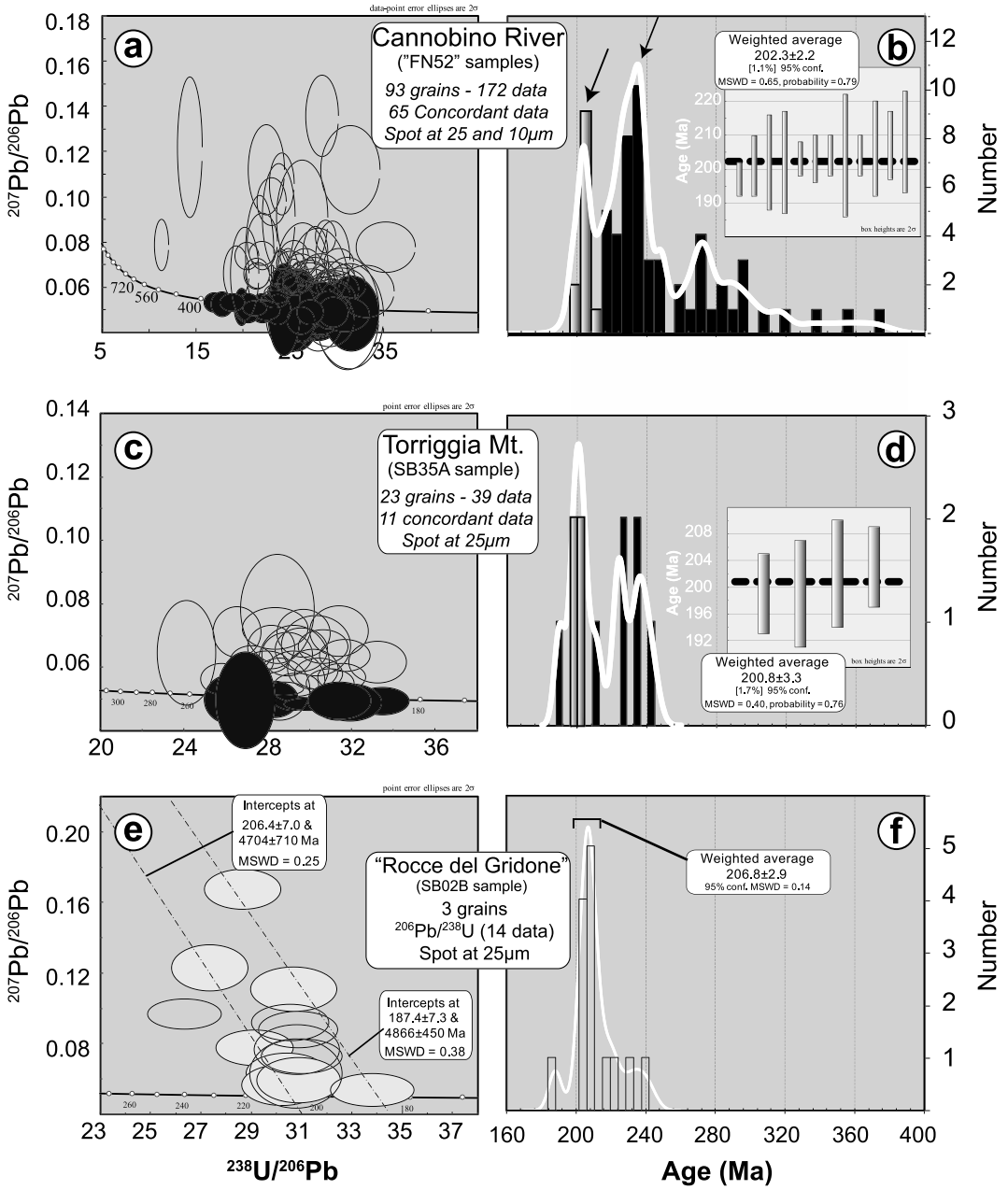

Figure 9. (left column; a, c, and e) Tera-Wasserburg diagrams of zircon U-Pb data: black ellipses refer to concordant data. In Figure 9e, two discordia lines with related intercepts are reported. (right column; b, d, and f) Probability density plots of (b and d) concordant data and (f) $^{206}Pb/^{238}U$ dates obtained from the different localities. The weighted averages of concordant U-Pb data obtained from the homogeneous grains/domains are reported for the Cannobino River and the Torriggia Mt. samples. Black arrows in Figure 9b indicate the two main clusters.

242 ± 9 Ma (Figures 9c and 9d). Four dates at 199 ± 6, 199 ± 8, 202 ± 8, and 203 ± 6 Ma were obtained from rims/domains of zircon grains within the matrix and showing homogeneous CL features (e.g., Zrc2 and Zrc18 in Figure 7). These data show a weighted average of 200.8 ± 3.3 Ma (MSWD = 0.40; Figure 9d). Triassic U-Pb concordant dates were obtained from zircon domains characterized by oscillatory zoning (e.g., Zrc15 and Zrc13 in Figure 7). The youngest U-Pb concordant date was obtained from the homogeneous rim of a zircon grain partially enclosed within garnet and showing the "cauliflower structure" (i.e., Zrc14 in Figure 7).

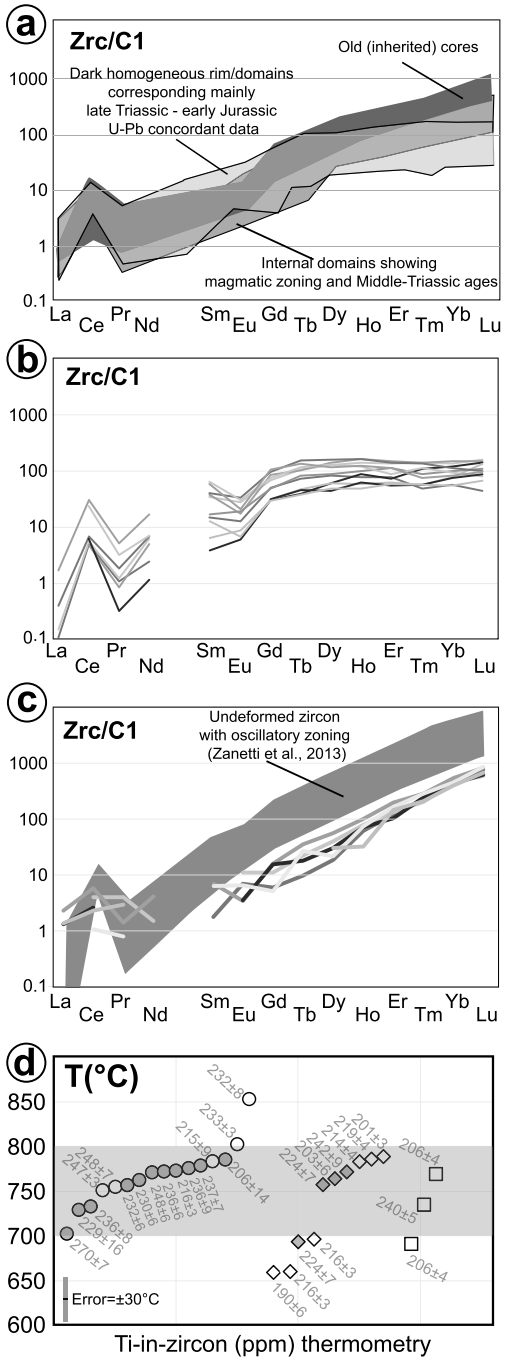

Figure 10. Chondrite (CI)-normalized (McDonough & Sun, 1995) REE patterns of different zircon domains from the different localities: (a) Cannobino River; (b) Torriggia Mt.; and (c) "Rocce del Gridone." The light-gray area in Figure 10c delimits REE patterns of undeformed zircon grains with oscillatory zoning from the External Gabbro unit analyzed by Zanetti et al. (2013). (d) Temperature estimates according to the Ti-in-zircon thermometry according to the calibration of Watson et al. (2006). Circles, diamonds, and squares refer to the Cannobino River, Torriggia Mt., and "Rocce del Gridone" samples, respectively. U-Pb concordant data (filled symbols) and $^{206}Pb/^{238}U$ dates (empty symbols) are reported with the 1σ error. The light-gray area delimits *T* estimates for zircon grains from the External Gabbro unit analyzed by Zanetti et al. (2013) by adopting the Ti-in zircon thermometry of Watson et al. (2006) with Ti content ranging from 7.35 to 16.7 ppm.

Zircon domains have a rather homogeneous trace element composition independent from their textures and U-Pb dates. The REE pattern is characterized by nearly flat HREE close to 100 times CI chondrite, as expected in a rock containing abundant garnet (Figures 3c, 3d, and 10b). LREEs are strongly depleted relative to HREEs and show a positive Ce anomaly. In most of the analyzed zircon, Eu shows a negative anomaly relative to the neighboring elements. The Th/U ratio is variable (0.55 and 2.8) and does not show any relationship with zircon texture (Table A1).

Zircon grains have a Ti content ranging from 3.64 to 16.85 ppm (10 data, Table A2), and the estimated temperatures vary from 659 to 789°C (Figure 10d).

6.1.3. "Rocce del Gridone" Outcrop

Three zircon grains were analyzed for the "Rocce del Gridone" sample (SB02B; Table A1) for a total of 14 analyses. U-Pb data are all discordant (Figure 9e), and the $^{206}Pb/^{238}U$ data range from 240 to 188 Ma with a major cluster (nine data) at about 206 Ma (weighted average = 206.8 ± 2.9 Ma, 95% conf. MSWD = 0.14; Figure 9f). Discordant data do not align (Figure 9e): however, two groups of data were calculated for discordia lines with lower and upper intercepts at 206.4 ± 7.0 Ma and 4,704 ± 710 Ma (MSWD = 0.25) and 187.4 ± 7.3 Ma and 4,866 ± 450 Ma (MSWD = 0.38), respectively (Figure 9e).

Zircons have fractionated REE patterns with HREE close to 1,000 times CI and LREE at about 1 times CI (Figure 10c). The positive Ce anomaly and the negative Eu anomaly are almost absent in the two large analyzed grains. The Th/U ratio is between 0.38 and 0.5 (Table A2).

Three values of Ti were obtained from Zrc1 and Zrc2 at 5.5, 9.3, and 13.58 ppm (Table A2), providing temperature estimates of 690, 735, and 768°C, respectively (Figure 10d).

6.2. Hf Isotopes

Nineteen zircon grains were analyzed for Hf isotopic composition, including a duplicate analysis of a homogeneous rim on one grain, giving a total of 20 analyses (Table A3). Zircon grains were selected based on CL features and U-Pb data. We mainly focused on cores showing magmatic features and with Triassic concordant dates and external homogeneous rims, which provided the weighted average of concordant data at 202.3 ± 2.2 Ma. In particular, we analyzed core domains with sector zoning (n = 2), oscillatory zoning (n = 2), and homogeneous CL texture (n = 7). In addition, analyses of rim domains with homogeneous CL texture included rims around sector zoned cores (n = 2), rims around oscillatory zoned cores (n = 3), and rims around homogeneous CL cores (n = 4). The initial $^{176}Hf/^{177}Hf$ values range from 0.282633 to 0.282845, corresponding to εHf values of −0.49 to 7.67 (Figure 11a), depleted mantle model ages of 0.86–0.56 Ga, and crustal model ages of 1.28–0.78 Ga. The obtained data form a single population that covers a broad range and partially overlaps the εHf values obtained from zircon grains within a plumasitic/dioritic dyke that cuts the External Gabbro unit (Figures 11a and 11b; Langone et al., 2017). Measurements of the $^{176}Yb/^{176}Hf$ are very low (suggesting notably low REE content; see trace elements above) and range from 0.01048 to 0.00071, resulting in small errors propagated from the correction for REE mass overlap.

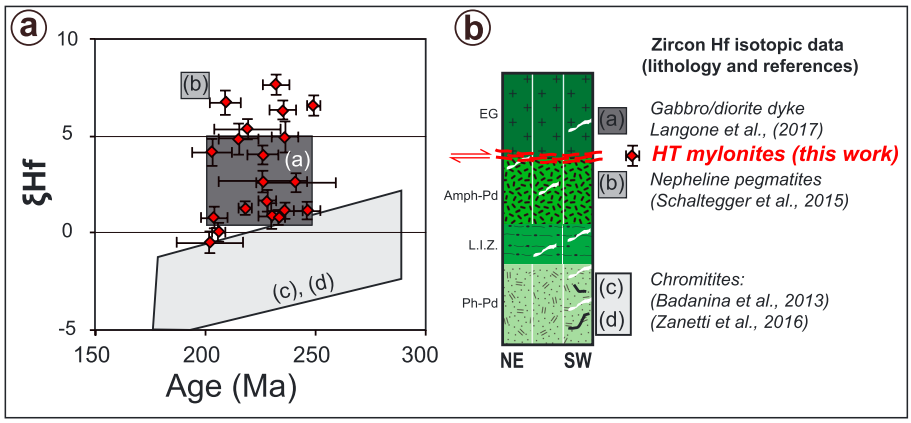

Figure 11. (a) εHf(*t*) versus U-Pb age for the zircon grains from the shear zone. Literature data of zircon from a dioritic dyke from the External Grabbro unit ((a); Langone et al., 2016, 2017); zircons from miaskite-type nepheline pegmatites in the Finero mafic complex ((b); Schaltegger et al., 2015); and zircon from chromitites within the mantle peridotites of Finero ((c) and (d); Badanina et al., 2013; Zanetti et al., 2016). (b) Schematic section (not to scale) of the mafic/ultramafic sequence of Finero showing the location in the schematic section and from NE to SW of the data.

7. Discussion

7.1. Metamorphic Evolution of the Shear Zone: A View From Mineral Assemblages and General Microstructures

The diverse mineral assemblages and microstructures observed within the (ultra)mylonites indicate a large range of *P-T* conditions of deformation (e.g., Daczko et al., 2002) and possible open system metasomatism of the gabbroic precursor rocks to form hornblendite (e.g., Daczko et al., 2016). Ductile deformation overprinted a high-*T* igneous and/or granulite facies mineral assemblage (amphibole, plagioclase, two pyroxenes, and garnet; Figures 4a–4f). The synkinematic development of new amphibole, plagioclase, and minor pyroxenes is indicative of amphibolite facies conditions of deformation (i.e., $T > 650$°C and $P < 0.4$–0.6 GPa; Degli Alessandrini et al., 2016). Mylonitic deformation was probably protracted or was at least reactivated at lower temperature conditions as suggested by the local occurrence of texturally late biotite, actinolite, and albite along the foliation planes (Figure 4c). The metamorphic history ended with the local development of chlorite, epidote, and albite at the expense of amphibole, pyroxenes, garnet, and plagioclase (e.g., Figure 4e). The deformation features of the studied mylonitic/ultramylonitic shear zone have been previously described by Kenkmann (2000), Kenkmann and Dresen (2002), and Degli Alessandrini et al. (2016). According to these authors, the localization of deformation at the margin of porphyroclasts increases reaction kinetics supporting amphibole and clinopyroxene replacement reactions (Kenkmann, 2000). Preliminary results obtained by Degli Alessandrini et al. (2016) led the authors to suggest that the synkinematic development of symplectites (e.g., Figure 4d) played an important role in grain size reduction, phase mixing within the matrix and strain localization.

7.2. Zircon: Origin, Microstructures, and Chemical Features

Zircon grains are anomalously abundant within the studied mafic/ultramafic mylonites and ultramylonites, including a major occurrence of zircon in mylonitic hornblendite layers. Moreover, zircon grains from the garnet-bearing metahornblendite tend to be, on average, larger than zircon grains from the other compositional bands in the shear zone, that is, meta-diorite/gabbro. For the mafic bulk composition of the rocks that host these zircons, such high abundance of zirconium (up to 259 ppm for the Cannobino River outcrop; Stähle et al., 2001) is unusual (e.g., Zr contents in other well-studied lower crustal gabbroic gneisses are typically <10–50 pmm; Schröter et al., 2004; Stuart et al., 2016, 2017). This anomaly suggests significant crustal contamination and inheritance during deformation as already suggested by Zanetti et al. (2013) and observed in deep crustal mafic plutonic rocks in other settings (e.g., Milan et al., 2016, 2017). The broad range of U-Pb dates and zircon internal CL textures support this hypothesis. A likely source of the xenocrysts includes lower crustal metasedimentary rocks of the structurally uppermost Kinzigite Formation (Hingerl et al., 2008; Lu et al., 1997; Stähle et al., 2001; Zanetti et al., 2013) that is locally enclosed within the mafic rocks

(i.e., the septa) and/or by older mafic intrusive rocks predating the Triassic ones of the External Gabbro unit (e.g., Langone et al., 2017). The large variation of the εHf values from −0.49 to 7.67 is unlikely to be related to the disturbance of the U-Pb system (as U, Pb, and Hf isotopes are decoupled; e.g., Halpin et al., 2012, 2013; Milan et al., 2016) and is more consistent with the occurrence of different zircon populations/sources, as suggested above.

U-Pb data include mainly discordant analyses with only 38% of analyses giving concordant dates for the Cannobino River and Torriggia Mt. outcrops and all analyses being discordant data for the "Rocce del Gridone" sample (Figure 9). The common occurrence of discordant U-Pb data is likely related to two main factors, that is, inheritance and crystal-plastic deformation. According to CL features and U-Pb data, zircon grains are of different origin: they occur as inherited grains from the metasedimentary sequence (i.e., Kinzigitic Formation), or they show magmatic features related to both Permian and Triassic events (e.g., Langone et al., 2017; Zanetti et al., 2013). Both types experienced metamorphic overprints and intense mylonitic deformation with local crystallization/recrystallization. Prior to deformation in the shear zones, the host rocks experienced multiple magmatic events, metasomatism (Langone et al., 2017), and metamorphic overprints (e.g., Kenkmann, 2000). All these events may have concurred to local Pb loss within zircon grains explaining, in part, discordance of inherited zircon grains.

Moreover, according to several authors, deformation can be a major cause of discordant U-Pb data (e.g., Moser et al., 2009; Piazolo et al., 2016; Piazolo et al., 2012; Timms et al., 2006). These authors show that intracrystalline deformation of zircon can occur at amphibolite-facies metamorphic conditions and can severely modify trace element geochemistry and isotopic composition, hence, age determination. Another common feature observed for zircon (both in thin section and as separates) is the occurrence of fractures with or without displacement. These brittle features have been observed for zircon grains within the matrix and included within porphyroclasts (garnet, amphibole, and pyroxene). We noted that zircon grains included within the porphyroclasts are generally located at the external portions of them. Porphyroclasts are crosscut by numerous fractures that also intersect the included zircon grains, defining a connection with the matrix. Moreover, porphyroclasts show evidence of both reaction and deformation (e.g., asymmetric reaction coronas) at their margin (e.g., Degli Alessandrini et al., 2016; Kenkmann, 2000). Therefore, brittle deformation concurred with ductile deformation in modifying the chemistry and isotopic composition of zircon grains. However, electron backscatter diffraction analysis of zircon grains is needed to characterize in detail intracrystalline deformation features and their link with chemical and isotopic data. The trace element composition and isotopic analyses of zircon grains from the studied shear zone reveal a notably lower HREE content (Figure 10; $<$1,000 times CI) than those reported in magmatic zircon grains from the weakly deformed/undeformed External Gabbro unit from the Cannobina valley (1,000 $<$ Zrc/CI $<$ 10,000; Zanetti et al., 2013; Figure 10c). This suggests that either the studied mylonites/ultramylonites derived from different precursor rocks (protoliths) compared to those studied and dated by Zanetti et al. (2013) or that fluid-present deformation modified (lowering) the REE content of zircon grains within the shear zone. Our field and petrographic observations, mineral chemistry, and isotopic data support the latter hypothesis. It is interesting to note that the REE profiles of the recrystallized rims/domains, with U-Pb concordant dates in the range of 206–190 Ma, are characterized by flatter HREE patterns with respect to the patterns obtained from zircon grain/domains showing magmatic zoning and older U-Pb data (Figure 10a). This suggests that the growth of these domains occurred in the presence of garnet or from HREE depleted fluids (most likely melts). According to Degli Alessandrini et al. (2016), during deformation, garnet underwent fracturing or reacted to produce plagioclase + orthopyroxene symplectite. The zircon rims/domains providing young concordant U-Pb data (about 202 and 206 Ma) are inconsistent with scavenging HREE during garnet breakdown (i.e., enrichment of the HREE in new zircon), suggesting that symplectite textures likely postdate zircon rim growth.

The application of the Ti-in-zircon thermometer provided temperature estimates mainly in the range of about 750 to 800°C (19 of 28 data; Figure 10d). This interval covers the *T* estimates calculated for both magmatic and recrystallized zircon grains from the External Gabbro unit (Figure 10d) by using the Ti-in-zircon thermometry and Ti values in the range of 7.35 and 16.7 ppm as reported in Zanetti et al. (2013). Temperature estimates obtained in this work probably indicate zircon crystallization from melts and/or the regional granulite facies metamorphism. Only for two homogeneous rims providing Late Triassic to Early Jurassic concordant data, the Ti content was measured and the Ti-in zircon thermometry applied (Figure 10d). The obtained temperatures at 790 and 764°C are like those obtained from the magmatic and inherited domains/grains. The scarcity of

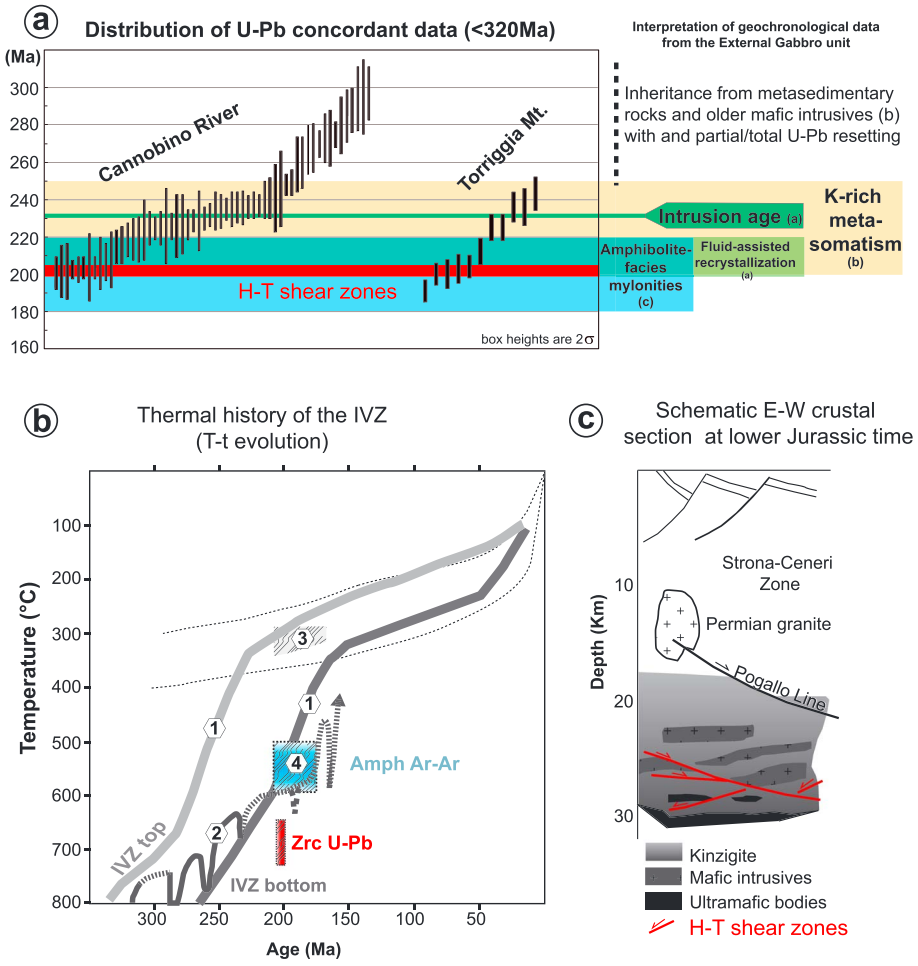

Figure 12. (a) Distribution plot of zircon U-Pb concordant data from the Cannobino River and Torriggia Mt. samples. Black vertical bars are U-Pb concordant dates (with associated 2σ error); red horizontal bar encloses the weighted average ages of deformation calculated from U-Pb concordant data of recrystallized zircon grains/domains. Literature geochronological data for the External Gabbro unit are from Zanetti et al. (2013; (a)), intrusion and fluid-assisted recrystallization; Langone et al. (2017; (b)), multiple-stage intrusion of the External Gabbro unit and K-rich metasomatism; and Boriani and Villa (1997; (c)), amphibolite-facies ductile deformation. (b) Temperature-time (*T-t*) diagram of different sectors of the Ivrea-Verbano Zone. The dark gray *T-t* paths for the bottom of the IVZ are from Siegesmund et al. (2008; 1) and Ewing et al. (2015; 2). The *T-t* path for the top of the IVZ is from Siegesmund et al. (2008). The light-gray *T-t* polygon (3) delimits the deformation temperatures of the Pogallo Line during its activity (Wolff et al., 2012). The thin dashed lines delimit the *T-t* exhumation path of the Pogallo mylonites (after Wolff et al., 2012). The red and light blue polygons delimit the *T-t* conditions for ductile deformation within the external gabbro unit according to LA-ICP-MS U-Pb dating (this work) and hornblende Ar-Ar dating (4; Boriani & Villa, 1997). Temperature of HT deformation is inferred from Ti-in-zircon thermometry and from literature (e.g., Degli Alessandrini et al., 2016); for the timing, we used the weighted average of U-Pb concordant dates of the recrystallized zircon grains/domains. (c) Schematic crustal section of the lower Jurassic passive continental margin in the Southern Alps (after Schmid et al., 1987, and Brodie & Rutter, 1987), showing extensional faults at different crustal levels in which activity was coeval.

Ti-in-zircon data from recrystallized domains does not allow constraining the temperature of deformation. However, our observations indicate that deformation occurred at amphibolite facies conditions with local recrystallization of zircon at *T* higher than 650°C, as already suggested by other authors (Degli Alessandrini et al., 2016; Kenkmann, 2000).

7.3. Timing of Deformation

Except for the Cannobino River samples, where an older component was detected, U-Pb concordant data are mainly distributed in the range of 240–190 Ma (Figures 9b, 9d, and 12a). According to recent zircon U-Pb data, the External Gabbro unit shows a complex evolution with evidence for magmatism from the Carboniferous to

Triassic and metasomatism during the Early/Middle Triassic (e.g., Langone et al., 2017). The U-Pb data obtained in this work do not elucidate the magmatic history of the External Gabbro further, but this was not the aim of our study. Instead, combining U-Pb data with microstructures and geochemical and CL features of zircon grains, we provide new temporal constraints on the post-magmatic history of the External Gabbro. The U-Pb concordant data of zircon grains from the Cannobino River outcrop define two main clusters at about 230 and 202 Ma. The Middle Triassic concordant data obtained from zircon grains showing internal magmatic features (i.e., oscillatory and sector zoning) can be linked to the Triassic magmatic activity recorded by the External Gabbro unit (e.g., Zanetti et al., 2013). Middle Triassic U-Pb concordant data were also obtained from rims around older cores (i.e., Early Triassic to Permian). These dates indicate crystallization/recrystallization during the Middle Triassic (Langone et al., 2017). We suggest that high-temperature deformation (>650°C), with zircon crystallization/recrystallization, occurred during the Late Triassic to Early Jurassic (weighted average of concordant data at 202 ± 2 and 201 ± 3 Ma; lower intercepts at 206 ± 7 and 187 ± 7 Ma; Figure 9), as mainly documented by the dark and homogeneous zircon rims and/or large structureless zircon grains/domains (e.g., Figures 5–7, and 9). Combining our results with existing geochronological data, the shear zone activity is inferred to have been long-lived: the high temperature (HT) deformation history recorded at the Triassic-Jurassic boundary continued at lower-grade metamorphic conditions during the Early Jurassic as suggested by amphibolite to greenschist facies mineral assemblages and by Ar-Ar dating of hornblende (mylonitic hornblende from the External Gabbro unit at 183 Ma; Boriani & Villa, 1997; Figures 12a and 12b).

7.4. Large-Scale Tectonic Link Between High-Temperature Deformation and Midcrustal Deformation

Based on concordant ages of recrystallized zircon rims/domains, the shear zone was active at HT conditions during the Late Triassic to Early Jurassic. This coincides with the activity of the Pogallo Line (210–170 Ma; Zingg et al., 1990; Mulch, Rosenau, et al., 2002; Mulch, Cosca, et al., 2002; Wolff et al., 2012), a crustal scale extensional fault zone with metamorphic conditions and deformation regime changing from ductile, toward the north, to brittle, toward the south (Handy, 1987). Wolff et al. (2012) provided a detailed reconstruction of the tectono-thermal evolution along the Pogallo Line. According to Wolff et al. (2012), the shear zone was active in a range of temperatures from 290 to 350°C, in the Val Cannobina and Val Pogallo, and at lower temperatures (220–310°C) further to the south (Val d'Ossola and Val Strona). Based on our new findings and existing thermo- and geochronological studies, extensional shearing occurred simultaneously at different crustal levels within the studied sector of the IVZ (Figure 12b). Detailed *T-t* reconstruction for the northern sector of the IVZ are lacking; thus, the *T-t* estimates for the lower crustal deformation in this sector can be compared with the available detailed *T-t* paths reconstructed for the central and southern sectors of the IVZ (Siegesmund et al., 2008; Ewing et al., 2015; Figure 12b). According to Siegesmund et al. (2008), the post-Permian cooling rate of the bottom and the top of the IVZ of the Val Strona di Omegna profile (central IVZ) was fast until Middle Jurassic, after which it became slow. These authors suggested that the deepest part of the crustal section experienced relatively high-temperature conditions (>550°C) at least until the Triassic (Figure 12b) and that at circa 210 Ma (hornblende Ar-Ar isochron ages) cooling and exhumation affected the deepest portions of the crustal profile pointing to the beginning of extension-induced subsidence in the upper crust (i.e., the Lombardian basin). Jurassic heating related to extensional tectonics was suggested by several authors based on U-Pb rutile dating of granulites (Ewing et al., 2015; Smye & Stockli, 2014). According to Beltrando et al. (2015), the time interval from the Middle Triassic to Early Jurassic was characterized by several stages of extensional faulting responsible for rift localization in a fossil rifted margin belonging to the Adriatic microplate. New thermochronological data (U-Th)/He ages in detrital zircons) allowed these authors to suggest that the future western edge of the Adriatic microplate recorded a localized heating-cooling cycle at 215–200 Ma together with the influx of mantle-derived fluids/melts. This time interval was further characterized by rift-related shearing at lower crustal levels slightly predating deformation within the upper crust (Beltrando et al., 2015, and references therein). The lower crustal shear zone studied in this work fits well within this framework, accommodating lower crustal extension, probably in response to the rifting processes at the Adriatic microplate, during the Late Triassic to Early Jurassic.

8. Conclusions

1. The studied high-temperature shear zone developed in the mafic metamorphic rocks of the External Gabbro unit. It broadly corresponds to the contact between the External Gabbro unit and the

Amphibole Peridotite unit of the Finero Mafic Complex. According to the present stratigraphic reconstruction, the studied shear zone can represent the deepest near-horizontal regional fault of the Ivrea-Verbano Zone (e.g., Schaltegger & Brack, 2007), possibly responsible for the exhumation of the mantle body and of the deeper crustal mafic-ultramafic sequence of the Finero Complex in Late Jurassic times (Zanetti et al., 2016).

2. Zircon is a common accessory mineral within mylonites and ultramylonites, and it occurs preferentially within the garnet-bearing meta-hornblenditic layers. Zircon has considerable dimensions (up to 500 μm) and generally shows rounded shapes and/or lobate contours. BSE-CL images reveal that zircon grains are homogeneous or they show complex internal features consisting of cores with oscillatory or sector zoning surrounded by homogeneous rims.
3. The U-Pb dating of several zircon grains analyzed both as separates and directly on thin section yield mainly discordant data. U-Pb dating and zircon internal features suggest a large component of inheritance from the country rocks, as already reported in literature (i.e., Zanetti et al., 2013), and a common occurrence of zircon grains or domains (e.g., cores) of magmatic origin survived mylonitization of the host rocks. The new results suggest that deformation with local zircon recrystallization occurred at the Triassic-Jurassic boundary (202 ± 4 Ma = weighted average of concordant U-Pb data from zircon rims from both the Cannobino River and Torriggia Mt. outcrops). HT shearing was partially coeval with fluid-assisted recrystallization within the weakly deformed metabasites of the External Gabbro unit (Zanetti et al., 2013) and slightly predated amphibolite-facies deformation as documented by hornblende Ar-Ar dating of mylonites (Boriani & Villa, 1997).
4. The studied lower crustal shear zone is comparable in terms of *P-T* conditions of deformation, kinematics, and composition to other high-grade shear zones exposed along the IVZ (i.e., Brodie & Rutter, 1987; Rutter et al., 1993). Geochronological data suggest that the studied shear zone was active coevally with other extensional shear zones that developed at shallower crustal levels (i.e., Pogallo Line). We report for the first time U-Pb zircon dating of lower crustal HT mylonitic deformation at the Triassic-Jurassic boundary, as previously suggested by Beltrando et al. (2015). According to Beltrando et al. (2015), ductile deformation at both lower and upper crustal levels should have played a fundamental role during the Triassic-Jurassic exhumation of the western paleomargin of Adria.

Acknowledgments

This work was funded by the MIUR PRIN 2015 (20158A9CBM) "Geochemical and isotopic budget of highly metasomatised sub-continental mantle in the Africa and Europe geodynamic systems: Modern and fossil analogues." Silvano Sinigoi and an anonymous reviewer are thanked for the constructive reviews of the manuscript. We would like to also thank the Associate Editors of this Special Volume in memory of our friend and colleague Marco Beltrando. The students Michela Grammatica, Beatrice Guarischi, Andrea Bonzani, and Matteo Stelitano provided generous support during mapping, sample preparation, and chemical and isotopic analyses. This is contribution 1013 from the ARC Centre of Excellence for Core to Crust Fluid Systems (http://www.ccfs.mq.edu.au) and 1182 in the GEMOC Key Centre (http://www.gemoc.mq.edu.au). The Hf analytical data were obtained using instrumentation funded by the DEST Systemic Infrastructure Grants, ARC LIEF, NCRIS/AuScope, industry partners, and Macquarie University. The data used for the present manuscript are listed in the appendixes (supporting information).

References

Badanina, I. Yu., Malitch, K. N., & Belosova, E. A. (2013). U-Pb and Hf isotope characteristics of zircon from chromitites at Finero. *Goldschmidt2013 Conference Abstracts, 683*.

Barboza, S. A., & Bergantz, G. W. (2000). Metamorphism and anatexis in the mafic complex contact aureole, Ivrea Zone, northern Italy. *Journal of Petrology*, *41*(8), 1307–1327. https://doi.org/10.1093/petrology/41.8.1307

Barboza, S. A., Bergantz, G. W., & Brown, M. (1999). Regional granulite facies metamorphism in the Ivrea Zone: Is the Mafic Complex the smoking gun or red herring? *Geology*, *27*(5), 447–450. https://doi.org/10.1130/0091-7613(1999)027%3C0447:RGFMIT%3E2.3.CO;2

Beltrando, M., Stockli, D. F., Decarlis, A., & Manatschal, G. (2015). A crustal-scale view at rift localization along the fossil Adriatic margin of the Alpine Tethys preserved in NW Italy. *Tectonics*, *34*, 1927–1951. https://doi.org/10.1002/2015TC003973

Berra, F., Galli, M. T., Reghellin, F., Torricelli, S., & Fantoni, R. (2009). Stratigraphic evolution of the Triassic-Jurassic succession in the western Southern Alps (Italy): The record of the two-stage rifting on the distal passive margin of Adria. *Basin Research*, *21*, 335–353. https://doi.org/10.1111/j.1365-2117.2008.00384.x

Bertotti, G., Picotti, V., Bernoulli, D., & Castellarin, A. (1993). From rifting to drifting: Tectonic evolution of the South Alpine upper crust from Triassic to Early Cretaceous. *Sedimentary Geology*, *86*(1-2), 53–76. https://doi.org/10.1016/0037-0738(93)90133-P

Boriani, A., & Burlini, L. (1995). Carta geologica della Valle Cannobina. Scala 1:25000. Comunità montana Valle Cannobina, Dipartimento di Scienze della Terra dell'Università degli Studi di Milano, Centro di Studio per la geodinamica Alpina e Quaternaria del CNR-Milano. Grafiche Diodoro, Milano.

Boriani, A. C., & Villa, I. M. (1997). Geochronology of regional metamorphism in the Ivrea-Verbano Zone and Serie dei Laghi, Italian Alps. *Schweizerische Mineralogische und Petrographische Mitteilungen*, *77*, 381–401.

Boriani, A., Burlini, L., & Sacchi, R. (1990). The Cossato-Mergozzo-Brissago Line and the Pogallo Line (Southern Alps, northern Italy) and their relationships with the late-Hercynian magmatic and metamorphic events. *Tectonophysics*, *182*(1-2), 91–102. https://doi.org/10.1016/0040-1951(90)90344-8

Brodie, K. H., & Rutter, E. H. (1987). Deep crustal extensional faulting in the Ivrea Zone of northern Italy. *Tectonophysics*, *140*(2-4), 193–212. https://doi.org/10.1016/0040-1951(87)90229-0

Brodie, K. H., Rex, D., & Rutter, E. H. (1989). On the age of deep crustal extensional faulting in the Ivrea Zone, northern Italy, alpine tectonics. *Geological Society - Special Publications*, *45*(1), 203–210. https://doi.org/10.1144/GSL.SP.1989.045.01.11

Daczko, N. R., Klepeis, K. A., & Clarke, G. L. (2002). Thermo-mechanical evolution of the crust during convergence and deep crustal pluton emplacement in the western province of Fiordland, New Zealand. *Tectonics*, *21*(4), 1022. https://doi.org/10.1029/2001TC001282

Daczko, N. R., Piazolo, S., Meek, U., Stuart, C. A., & Elliott, V. (2016). Hornblendite delineates zones of mass transfer through the lower crust. *Scientific Reports*, *6*(1), 1–6, 31369. https://doi.org/10.1038/srep31369

Degli Alessandrini, G., Menegon, L., Beltrando, M., Gijkstra, A., & Anderson, M., (2016). Metamorphic reactions, grain size reduction and deformation of mafic lower crustal rocks. Geophysical Research Abstracts 18, EGU2016-13587, 2016 EGU General Assembly 2016.

Demarchi, G., Quick, J. E., Sinigoi, S., & Mayer, A. (1998). Pressure gradient and original orientation of a lower-crustal intrusion in the Ivrea–Verbano Zone, northern Italy. *The Journal of Geology*, *106*(5), 609–622. https://doi.org/10.1086/516045

Ewing, T. A., Rubatto, D., Beltrando, M., & Hermann, J. (2015). Constraints on the thermal evolution of the Adriatic margin during Jurassic continental break-up: U–Pb dating of rutile from the Ivrea–Verbano Zone, Italy. *Contributions to Mineralogy and Petrology*, *169*(4). https://doi.org/10.1007/s00410-015-1135-6

Fountain, D. M. (1976). Ivrea–Verbano and Strona–Ceneri zones, northern Italy—Cross section of continental crust—New evidence from seismic velocities of rock samples. *Tectonophysics*, *33*(1-2), 145–165. https://doi.org/10.1016/0040-1951(76)90054-8

Grieco, G., Ferrario, A., Von Quadt, A., Koeppel, V., & Mathez, E. A. (2001). The zircon-bearing chromitites of the phlogopite peridotite of Finero (Ivrea Zone, Southern Alps): Evidence and geochronology of a metasomatized mantle slab. *Journal of Petrology*, *42*(1), 89–101. https://doi.org/10.1093/petrology/42.1.89

Griffin, W. L., Belousova, E. A., Shee, S. R., Pearson, N. J., & O'Reilly, S. Y. (2004). Archean crustal evolution in the northern Yilgarn craton: U–Pb and Hf-isotope evidence from detrital zircons. *Precambrian Research*, *131*(3-4), 231–282. https://doi.org/10.1016/j.precamres.2003.12.011

Griffin, W. L., Pearson, N. J., Belousova, E. A., & Saeed, A. (2007). Reply to "Comment to short-communication 'Comment: Hf-isotope heterogeneity in zircon 91500' by Griffin, W.L., Pearson, N.J., Belousova, E.A., Saeed, A. (Chem Geol 233:358–363 2006)" by Corfu F. *Chemical Geology*, *244*(1-2), 354–356. https://doi.org/10.1016/j.chemgeo.2007.06.023

Halpin, J. A., Daczko, N. R., Milan, L. A., & Clarke, G. L. (2012). Decoding near-concordant U–Pb zircon ages spanning several hundred million years: Recrystallisation, metamictisation, or diffusion? *Contributions to Mineralogy and Petrology*, *163*(1), 67–85. https://doi.org/10.1007/s00410-011-0659-7

Halpin, J. A., Daczko, N. R., Clarke, G. L., & Murray, K. R. (2013). Basin analysis in polymetamorphic terranes: An example from east Antarctica. *Precambrian Research*, *231*, 78–97. https://doi.org/10.1016/j.precamres.2013.03.015

Handy, M. R. (1987). The structure, age and kinematics of the Pogallo fault zone-Southern Alps, northwestern Italy. *Eclogae Geologicae Helvetiae*, *80*, 593–632.

Handy, M. R., Franz, L., Heller, F., Janott, B., & Zurbriggen, R. (1999). Multistage accretion and exhumation of the continental crust (Ivrea crustal section, Italy and Switzerland). *Tectonics*, *18*(6), 1154–1177. https://doi.org/10.1029/1999TC900034

Henk, A., Franz, L., Teufel, S., & Oncken, O. (1997). Magmatic underplating, extension and crustal reequilibration: Insights from a cross-section through the Ivrea Zone and Strona-Ceneri Zone, northern Italy. *Journal of Geology*, *105*, 367–377.

Hiess, J., Condon, D. J., McLean, N., & Noble, S. R. (2012). $^{238}U/^{235}U$ systematics in terrestrial uranium bearing minerals. *Geology*, *335*, 1610–1614.

Hingerl, F., Klotzli, U., Steuber, C., & Kleinschrodt, R. (2008). New results from the mafic complex in the Finero area. 33th International Geological Congress, Oslo 6–14 August 2008, CDROM abstracts, X-CD Technologies. Retrieved from http://www.cprm.gov.br/33IGC/1344964.html

Hodges, K. V., & Fountain, D. M. (1984). Pogallo Line, South Alps, northern Italy: An intermediate crystal level, low-angle normal fault? *Geology*, *12*(3), 151–155. https://doi.org/10.1130/0091-7613(1984)12%3C151:PLSANI%3E2.0.CO;2

Horstwood, M. S. A., Foster, G. L., Parrish, R. R., Noble, S. R., & Nowell, G. M. (2003). Common-Pb corrected in situ U–Pb accessory mineral geochronology by LA–MC–ICP–MS. *Journal of Analytical Atomic Spectrometry*, *18*(8), 837–846. https://doi.org/10.1039/B304365G

Jackson, S. E., Pearson, N. J., Griffin, W. L., & Belousova, E. (2004). The application of laser ablation inductively coupled plasma mass spectrometry to in situ U–Pb zircon geochronology. *Chemical Geology*, *211*, 47–69. https://doi.org/10.1016/j.chemgeo.2004.06.017

Kenkmann, T. (2000). Processes controlling the shrinkage of porphyroclasts in gabbroic shear zones. *Journal of Structural Geology*, *22*(4), 471–487. https://doi.org/10.1016/S0191-8141(99)00177-7

Kenkmann, T., & Dresen, G. (2002). Dislocation microstructure and phase distribution in a lower crustal shear zone – An example from the Ivrea-zone, Italy. *International Journal of Earth Sciences (Geologische Rundschau)*, *91*(3), 445–458. https://doi.org/10.1007/s00531-001-0236-9

Ketchum, J. W. F., Jackson, S. E., Culshaw, N. G., & Barr, S. M. (2001). Depositional and tectonic setting of the Paleoproterozoic Lower Aillik Group, Makkovik Province, Canada: Evolution of a passive margin-foredeep sequence based on petrochemistry and U-Pb (TIMS and LAM-ICP-MS) geochronology. *Precambrian Research*, *105*(2-4), 331–356. https://doi.org/10.1016/S0301-9268(00)00118-2

Klotzli, U., Hochleitner, R., & Kosler, J. (2007). Lower Triassic mantle-derived magmatism in the Ivrea-Verbano Zone: Evidence from laser ablation U-Pb dating of a pegmatite from the eastern Finero Complex (Switzerland). *Mitteilungen der Osterreichischen Mineralogischen Gesellschaft*, *153*, 65.

Klötzli, U. S., Sinigoi, S., Quick, J. E., Demarchi, G., Tassinari, C. C. G., Sato, K., & Günes, Z. (2014). Duration of igneous activity in the Sesia Magmatic System and implications for high-temperature metamorphism in the Ivrea–Verbano deep crust. *Lithos*, *206–207*, 19–33.

Kretz, R. (1983). Symbol for rock-forming minerals. *American Mineralogist*, *68*, 277–279.

Langone, A., & Tiepolo, M. (2015). U–Th–Pb "multi–phase" approach to the study of crystalline basement: Application to the northernmost sector of the Ivrea–Verbano Zone (Alps). *Periodico di Mineralogia*, *84*, 633–655.

Langone, A., Padrón-Navarta, J. A., Ji W.-Q., Zanetti, A., Mazzucchelli, M., Tiepolo, M., … Bonazzi, M. (2016). Brittle-ductile deformation effects on zircon crystal-chemistry and U-Pb ages: An example from the Finero mafic complex (Ivrea-Verbano Zone, Western Alps). *Geophysical Research Abstracts* 18, EGU2016–6049, EGU General Assembly 2016.

Langone, A., Padrón-Navarta, J. A., Ji, W.-Q., Zanetti, A., Mazzucchelli, M., Tiepolo, M., … Bonazzi, M. (2017). Ductile-brittle deformation effects on crystal-chemistry and U-Pb ages of magmatic and metasomatic zircons from a dyke of the Finero mafic complex (Ivrea-Verbano Zone, Italian Alps). *Lithos*, *284-285*, 493–511. https://doi.org/10.1016/j.lithos.2017.04.020

Lu, M., Hofmann, A. W., Mazzucchelli, M., & Rivalenti, G. (1997). The mafic-ultramafic complex near Finero (Ivrea-Verbano Zone), I. Chemistry of MORB-like magmas. *Chemical Geology*, *140*(3-4), 207–222. https://doi.org/10.1016/S0009-2541(97)00049-1

Ludwig, K. R. (2003). *Isoplot/Ex Version 3.0: A Geochronological Toolkit for Microsoft Excel. Berkeley Geochronology Center Special Publication 4* (p. 70). Berkeley: Berkeley Geochronology Center.

McDonough, W. F., & Sun, S.-S. (1995). The composition of the Earth. *Chemical Geology*, *120*(3-4), 223–253. https://doi.org/10.1016/0009-2541(94)00140-4

Milan, L. A., Daczko, N. R., Clarke, G. L., & Allibone, A. H. (2016). Complexity of in-situ zircon U-Pb-Hf isotope systematics during arc magma genesis at the roots of a Cretaceous arc, Fiordland, New Zealand. *Lithos*, *264*, 296–314. https://doi.org/10.1016/j.lithos.2016.08.023

Milan, L. A., Daczko, N. R., & Clarke, G. L. (2017). Cordillera Zealandia: A Mesozoic arc flare-up on the palaeo-Pacific Gondwana margin. *Scientific Reports*, *7*, 261. https://doi.org/10.1038/s41598-017-00347-w, 1–9.

Moser, D. E., Davis, W. J., Reddy, S. M., Flemming, R. L., & Hart, R. J. (2009). Zircon U–Pb strain chronometry reveals deep impact-triggered flow. *Earth and Planetary Science Letters*, *277*, 73–79. https://doi.org/10.1016/j.epsl.2008.09.036

Mulch, A., Rosenau, M., Dörr, W., & Handy, M. R. (2002). The age and structure of dikes along the tectonic contact of the Ivrea-Verbano and Strona-Ceneri zones (Southern Alps, northern Italy, Switzerland). *Schweizerische Mineralogische und Petrographische Mitteilungen*, *82*, 55–76.

Mulch, A., Cosca, M. A., & Handy, M. R. (2002). In-situ UV-laser $^{40}Ar/^{39}Ar$ geochronology of a micaceous mylonite: An example of defect enhanced argon loss. *Contributions to Mineralogy and Petrology*, *142*(6), 738–752. https://doi.org/10.1007/s00410-001-0325-6

Pearce, N. J. G., Perkins, W. T., Westgate, J. A., Gorton, M. P., Jackson, S. E., Neal, C. R., & Chenery, S. P. (1997). A compilation of new and published major and trace element data for NIST SRM 610 and NIST SRM 612 glass reference materials. *Geostandards Newsletter*, *21*(1), 115–144. https://doi.org/10.1111/j.1751-908X.1997.tb00538.x

Peressini, G., Quick, J. E., Sinigoi, S., Hofmann, A. W., & Fanning, M. (2007). Duration of a large mafic intrusion and heat transfer in the lower crust: A SHRIMP U–Pb zircon study in the Ivrea-Verbano zone (Western Alps, Italy). *Journal of Petrology*, *48*, 1185–1218. https://doi.org/10.1093/petrology/egm014

Piazolo, S., Austrheim, H., & Whitehouse, M. (2012). Brittle-ductile microfabrics in naturally deformed zircon: Deformation mechanisms and consequences for U–Pb dating. *American Mineralogist*, *97*(10), 1544–1563. https://doi.org/10.2138/am.2012.3966

Piazolo, S., La Fontaine, A., Trimby, P., Harley, S., Yang, L., Armstrong, R., & Cairney, J. M. (2016). Deformation-induced trace element redistribution in zircon revealed using atom probe tomography. *Nature Communications*, *7*, 10490. https://doi.org/10.1038/ncomms10490

Redler, C., Johnson, T. E., White, R. W., & Kunz, B. E. (2012). Phase equilibrium constraints on a deep crustal metamorphic field gradient: Metapelitic rocks from the Ivrea Zone (NW Italy). *Journal of Metamorphic Geology*, *30*(3), 235–254. https://doi.org/10.1111/j.1525-1314.2011.00965.x

Rivalenti, G., Garuti, G., & Rossi, A. (1975). The origin of the Ivrea-Verbano basic formation (western Italian Alps); Whole rock geochemistry. *Bollettino della Società Geologica Italiana*, *94*, 1149–1186.

Rutter, E. H., Brodie, K. H., & Evans, P. (1993). Structural geometry, lower crustal magmatic underplating and lithospheric stretching in the Ivrea-Verbano Zone, N. Italy. *Journal of Structural Geology*, *15*(3-5), 647–662. https://doi.org/10.1016/0191-8141(93)90153-2

Rutter, E., Brodie, K., James, T., & Burlini, L. (2007). Large-scale folding in the upper part of the Ivrea-Verbano Zone, NW Italy. *Journal of Structural Geology*, *29*, 1–17. https://doi.org/10.1016/j.jsg.2006.08.013

Schaltegger, U., & Brack, P. (2007). Crustal-scale magmatic system during intracontinental strike-slip tectonics: U, Pb and Hf isotopic constraints from Permian magmatic rocks of the Southern Alps. *International Journal of Earth Sciences*, *96*, 1131–1151. https://doi.org/10.1007/s00531-006-0165-8

Schaltegger, U., Ulianov, A., Müntener, O., Ovtcharova, M., Vonlanthen, P., Vennemann, T., … Girlanda, F. (2015). Megacrystic zircon with planar fractures in miaskite-type nepheline pegmatites formed at high pressures in the lower crust (Ivrea Zone, Southern Alps, Switzerland). *American Mineralogist*, *100*(1), 83–94. https://doi.org/10.2138/am-2015-4773

Scherer, E., Münker, C., & Mezger, K. (2001). Calibration of the Lutetium-Hafnium clock. *Science*, *293*, 683–687.

Schmid, S. M. (1993). Ivrea zone and adjacent southern alpine basement. In J. F. von Raumer, & F. Neubauer (Eds.), *Pre-Mesozoic Geology in the Alps* (pp. 567–583). Berlin: Springer. https://doi.org/10.1007/978-3-642-84640-3_33

Schmid, R., & Wood, B. J. (1976). Phase relationships in granulitic metapelites from the Ivrea-Verbano Zone (northern Italy). *Contributions to Mineralogy and Petrology*, *54*(4), 255–279. https://doi.org/10.1007/BF00389407

Schmid, S. M., Zingg, A., & Handy, M. R. (1987). The kinematics of movements along the Insubric line and the emplacement of the Ivrea Zone. *Tectonophysics*, *135*(1-3), 47–66. https://doi.org/10.1016/0040-1951(87)90151-X

Schröter, F. C., Stevenson, J. A., Daczko, N. R., Clarke, G. L., Pearson, N. J., & Klepeis, K. A. (2004). Trace element partitioning during high-P partial melting and melt-rock interaction; An example from northern Fiordland, New Zealand. *Journal of Metamorphic Geology*, *22*, 443–457. https://doi.org/10.1111/j.1525-1314.2004.00525.x

Siegesmund, S., Layer, P., Dunkl, I., Vollbrecht, A., Steenken, A., Wemmer, K., & Ahrendt, H. (2008). Exhumation and deformation history of the lower crustal section of the Valstrona di Omegna in the Ivrea Zone, Southern Alps. In S. Siegesmund, B. Fügeschuh, & N. Froitzheim (Eds.), *Tectonic Aspects of the Alpine-Dinaride-Carpathian System*. *Geological Society of London, Special Publication, 298*, 45–68. https://doi.org/10.1144/SP298.3

Siena, F., & Coltorti, M. (1989). The petrogenesis of a hydrated mafic-ultramafic complex and the role of amphibole fractionation at Finero (Italian Western Alps). *Neues Jahrbuch für Mineralogie*, *6*, 255–274.

Sinigoi, S., Quick, J. E., Demarchi, G., & Peressini, G. (2010). The Sesia magmatic system. *Journal of the Virtual Explorer*, *36*. https://doi.org/10.3809/jvirtex.2010.00218

Smye, A. J., & Stockli, D. F. (2014). Rutile U–Pb age depth profiling: A continuous record of lithospheric thermal evolution. *Earth and Planetary Science Letters*, *408*, 171–182. https://doi.org/10.1016/j.epsl.2014.10.013

Stähle, V., Frenzel, G., Kober, B., Michard, A., Puchelt, H., & Schneider, W. (1990). Zircon syenite pegmatites in the Finero peridotite (Ivrea Zone): Evidence for a syenite from a mantle source. *Earth and Planetary Science Letters*, *101*(2-4), 196–205. https://doi.org/10.1016/0012-821X(90)90153-O

Stähle, V., Frenzel, G., Hess, J. C., Saupé, F., Schmidt, S. T., & Schneider, W. (2001). Permian metabasalt and Triassic alkaline dykes in the northern Ivrea zone: Clues to the post-Variscan geodynamic evolution of the Southern Alps. *Schweizerische Mineralogische und Petrographische Mitteilungen*, *81*, 1–21.

Stuart, C. A., Piazolo, S., & Daczko, N. R. (2016). Mass transfer in the lower crust: Evidence for incipient melt assisted flow along grain boundaries in the deep arc granulites of Fiordland, New Zealand. *Geochemistry, Geophysics, Geosystems*, *17*, 3733–3753. https://doi.org/10.1002/2015GC006236

Stuart, C. A., Daczko, N. R., & Piazolo, S. (2017). Local partial melting of the lower crust triggered by hydration through melt–rock interaction: An example from Fiordland, New Zealand. *Journal of Metamorphic Geology*, *35*(2), 213–230. https://doi.org/10.1111/jmg.12229

Timms, N. E., Kinny, P., & Reddy, S. M. (2006). Enhanced diffusion of uranium and thorium linked to crystal plasticity in zircon. *Geochemical Transactions*, *7*. https://doi.org/10.1186/1467-4866-7-10

Van Achterbergh, E., Ryan, C. G., Jackson, S. E., & Griffin, W. (2001). Data reduction software for LAICPMS. In P. Sylvester (Ed.), *Laser Ablation ICPMS in the Earth Sciences: Principles and Applications*, *Mineralogical Association of Canada Short Course Series* (Vol. 29, pp. 239–243). Québec City: Mineralogical Association of Canada.

Vavra, G., & Schaltegger, U. (1999). Post-granulite facies monazite growth and rejuvenation during Permian to Lower Jurassic thermal and fluid events in the Ivrea Zone (Southern Alps). *Contributions to Mineralogy and Petrology*, *134*(4), 405–414. https://doi.org/10.1007/s004100050493

Vavra, G., Schmid, R., & Gebauer, D. (1999). Internal morphology, habit and U–Th–Pb microanalysis of amphibolite-to-granulite facies zircons: Geochronology of the Ivrea Zone (Southern Alps). *Contributions to Mineralogy and Petrology*, *134*(4), 380–404. https://doi.org/10.1007/s004100050492

von Quadt, A., Ferrario, A., Diella, V., Hansmann, W., Vavra, G., & Koppel, V. (1993). U-Pb ages of zircons from chromitites of the phlogopite peridotite of Finero, Ivrea zone, N-Italy. *Schweizerische Mineralogische und Petrographische Mitteilungen*, *73*, 137–138.

Watson, E. B., Wark, D. A., & Thomas, J. B. (2006). Crystallization thermometers for zircon and rutile. *Contributions to Mineralogy and Petrology*, *151*, 413–433. https://doi.org/10.1007/s00410-006-0068-5

Wiedenbeck, M., Allé, P., Corfu, F., Griffin, W. L., Meier, M., Oberli, F., … Spiegel, W. (1995). Three natural zircon standards for U–Th–Pb, Lu–Hf, trace elements and REE analyses. *Geostandards Newsletter*, *19*(1), 1–23. https://doi.org/10.1111/j.1751-908X.1995.tb00147.x

Wolff, R., Dunkl, I., Kiesselbach, G., Wemmer, K., & Siegesmund, S. (2012). Thermochronological constraints on the multiphase exhumation history of the Ivrea-Verbano Zone of the Southern Alps. *Tectonophysics*, *579*, 104–117. https://doi.org/10.1016/j.tecto.2012.03.019

Zanetti, A., Mazzucchelli, M., Sinigoi, S., Giovanardi, T., Peressini, G., & Fanning, M. (2013). SHRIMP U–Pb zircon Triassic intrusion age of the Finero mafic complex (Ivrea–Verbano Zone, Western Alps) and its geodynamic implications. *Journal of Petrology*, *54*(11), 2235–2265. https://doi.org/10.1093/petrology/egt046

Zanetti, A., Giovanardi, T., Langone, A., Tiepolo, M., Wu, F.-Y., Dallai, L., & Mazzucchelli, M. (2016). Origin and age of zircon-bearing chromitite layers from the Finero phlogopite peridotite (Ivrea–Verbano Zone, Western Alps) and geodynamic consequences. *Lithos*, *262*, 58–74.

Zingg, A. (1983). The Ivrea and Strona-Ceneri zones (Southern Alps, Ticino and N-Italy) – A review. *Schweizer Mineralogische und Petrographische Mitteilungen*, *63*, 361–392.

Zingg, A., Handy, M. R., Hunziker, J. C., & Schmid, S. M. (1990). Tectonometamorphic history of the Ivrea Zone and its relationship to the crustal evolution of the Southern Alps. *Tectonophysics*, *182*(1-2), 169–192. https://doi.org/10.1016/0040-1951(90)90349-D